CrossMark

Little Ice Age wetting of interior Asian deserts and the rise of the Mongol Empire

Aaron E. Putnam [a, b, *], David E. Putnam [c], Laia Andreu-Hayles [b], Edward R. Cook [b], Jonathan G. Palmer [d], Elizabeth H. Clark [b], Chunzeng Wang [c], Feng Chen [e], George H. Denton [a], Douglas P. Boyle [f], Scott D. Bassett [f], Sean D. Birkel [a], Javier Martin-Fernandez [b], Irka Hajdas [g], John Southon [h], Christopher B. Garner [f], Hai Cheng [i], Wallace S. Broecker [b]

[a] School of Earth and Climate Sciences and Climate Change Institute, University of Maine, Orono, ME 04469, USA
[b] Lamont-Doherty Earth Observatory, 61 Rt. 9w, Palisades, NY 10964, USA
[c] College of Arts and Sciences, University of Maine at Presque Isle, Presque Isle, ME 04769, USA
[d] Climate Change Research Centre, School of Biological, Earth and Environmental Sciences, The University of New South Wales, Sydney, 2052 NSW, Australia
[e] Institute of Desert Meteorology, China Meteorological Administration, Ürümqi, China
[f] Department of Geography, University of Nevada, Reno, Reno, NV 89557-0154, USA
[g] Ion Beam Physics, ETH, Zürich, Switzerland
[h] School of Physical Sciences, University of California, Irvine, Irvine, CA 92697, USA
[i] Institute of Global Environmental Change, Xi'an Jiaotong University, Xi'an 710049, China

ARTICLE INFO

ABSTRACT

The degree to which warming of the planet will alter Asia's water resources is an important question for food, energy, and economic security. Here we present geological evidence, underpinned by radiometric dating and dendrochronology, and bolstered by hydrological modeling, indicating that wetter-than-present conditions characterized the core of the inner Asian desert belt during the Little Ice Age, the last major Northern Hemispheric cold spell of the Holocene. These wetter conditions accompanied northern mid-latitude cooling, glacier expansion, a strengthened/southward-shifted boreal jet, and weakened south Asian monsoons. We suggest that southward migration of grasslands in response to these wetter conditions aided the spread of Mongol Empire steppe pastoralists across Asian drylands. Conversely, net drying over the 20th century has led to drought that is unprecedented for the past ~830 years, and that could intensify with further heating of the Asian continent.

© 2015 Elsevier Ltd. All rights reserved.

1. Introduction

Sub-millennial climate fluctuations and associated changes in moisture availability can have important effects on human civilizations (Zhang et al., 2008; Buckley et al., 2010; Cook et al., 2010;

Pederson et al., 2014; Davi et al., 2015). Water-climate interactions are particularly important in Asia, Earth's largest and most populous continent, where hydroclimatic changes may have attended cultural shifts over the past two millennia (Zhang et al., 2008; Pederson et al., 2014). Although atmospheric temperatures over the center of the Asian continent are highly sensitive to radiative heating of the land surface (Solomon et al., 2007; McKinnon et al., 2013; McKinnon and Huybers, 2014), it is uncertain how the hydrological system will respond to future warming (Chiang

---

and Friedman, 2012; Broecker and Putnam, 2013). Here we present geomorphological, biological, and historical evidence for hydroclimatic change during the past ~830 yrs in the Tarim Basin of the inner Asian desert belt. Our reconstruction affords insight into relationships among climate change, water, and human culture in the heart of Asia, as well as how water resources might respond to future atmospheric warming.

The large (~1,090,000 km²) and closed Tarim Basin of western China (42-36°N, 74-95°E) is well positioned for monitoring hydrologic responses to climatic change in the mid-latitude deserts of interior Asia (Fig. 1). The Tarim Basin is bordered by the high Tien Shan, Pamir, and Kunlun ranges along its northern, western, and southern edges (Fig. 1). It features the Taklamakan Desert, the second-largest shifting-sand desert on Earth, as well as the Lop Desert, a now-dry eastern lakebed. Major drainage systems of the Tarim Basin include the Tarim, Yarkand, Khotan, Keriya, Niya, Aktash, Endere, Cherchen, and Konqi Rivers, all of which now terminate in the Taklamakan Desert (Yang et al., 2006). The Tarim,

Cherchen, and Konqi Rivers flow toward the Lop Desert, where in historical times there existed a large lake known as 'Lop Nor' ('Nor' is derived from the Mongolian word for 'Lake') (Li et al., 2008).

The surface elevation of the groundwater table in the Tarim Basin is modulated by rivers fed from spring/summer melt of winter snowpack in the high adjacent mountains, as well as by evaporation over the deserts (Yang et al., 2002; Chen et al., 2006b). Winter snow of the high mountain ranges alongside the Tarim Basin is nourished by orographic precipitation from strong westerly airflow, and is ablated by summer warmth. Thus temperature and atmospheric circulation are dominant controls on runoff (e.g., Aizen et al., 1995; Luce et al., 2014).

Landforms composed of waterlain sediments are widespread in the Taklamakan Desert (Yang et al., 2002, 2006), indicating higher-than-present groundwater surface elevations in the past. These landforms are wind-scoured platforms of laminated sand and silt overlain by shifting sand dunes meters to tens-of-meters in relief (Figs. 2 and 3; see also site descriptions below). In the Lop Desert, a
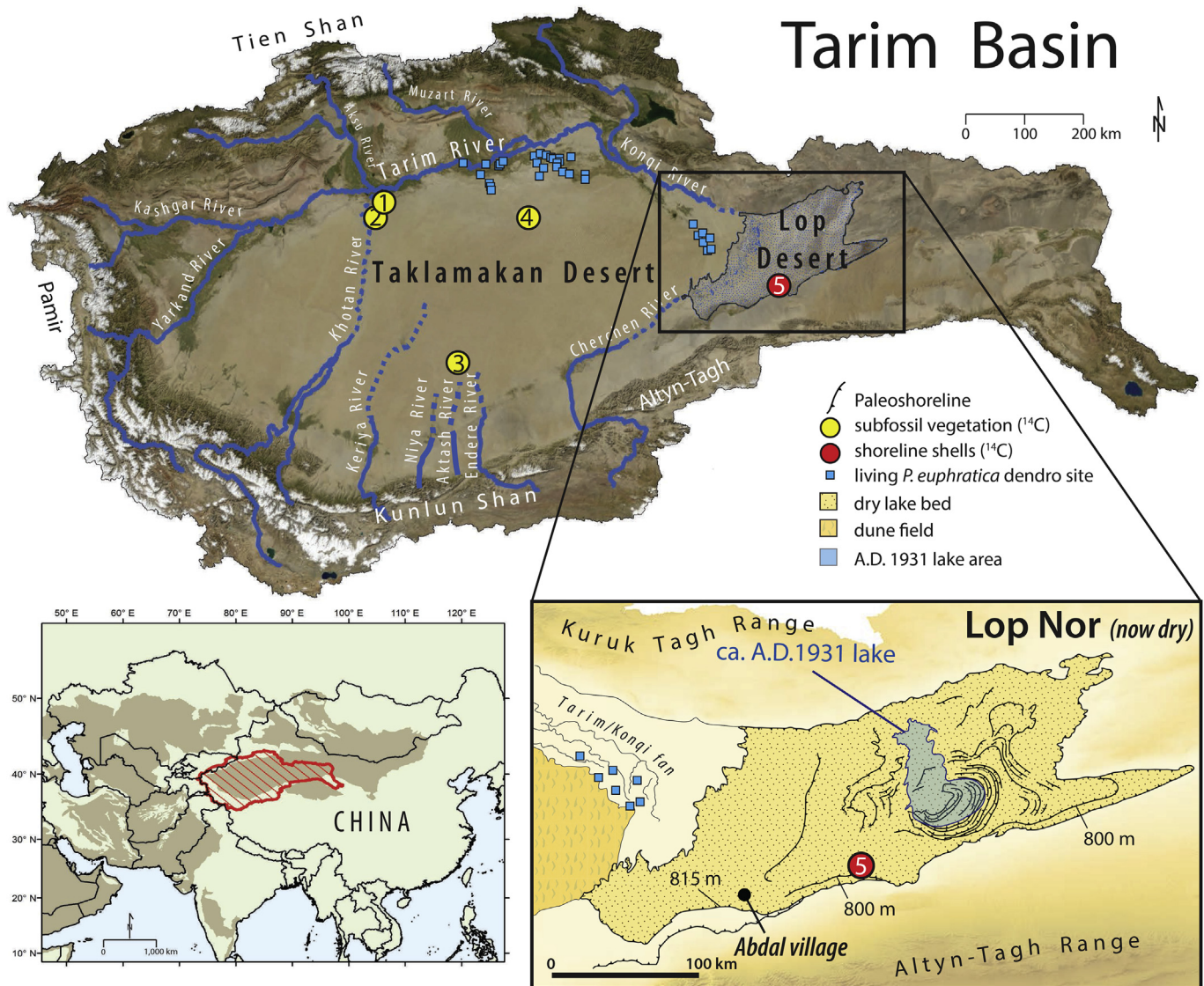
Fig. 1. Map of the Tarim Basin, western China. The Lop Desert is outlined in dark grey. Geomorphologic map of the Lop Desert region is enlarged. The A.D. 1931 lake margin (Hörner and Chen, 1935; Li et al., 2008) is shaded light blue. Solid blue lines show the Tarim Basin rivers. Dashed blue lines show riverbeds that today experience erratic (if any) flow. Eurasian context map is inset, with deserts shaded brown and the Tarim Basin perimeter outlined in red. (For interpretation of the references to color in this figure legend, the reader is referred to the web version of this article.)

Fig. 2. Photograph of wind-deflated, waterlain sedimentary platforms, partially overlain by migrating sand dunes, at Taklamakan Desert site 1 (Fig. 1). *P. euphratica* log in foreground corresponds to samples TD-10-08, and TD-14C-10.
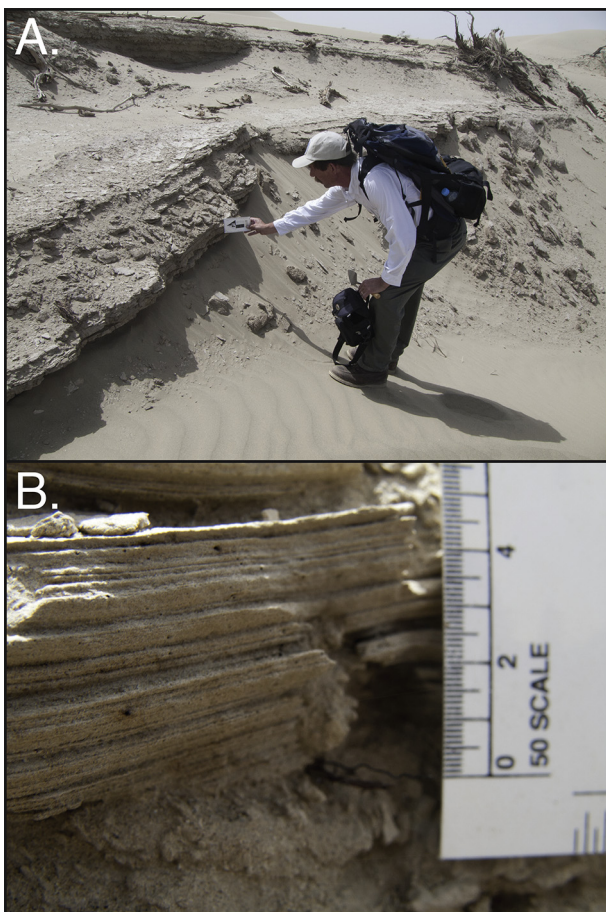
Fig. 3. Panel A: Photograph of eroded terrace composed of rhythmically laminated silty sands of Taklamakan Desert site 1 (Fig. 1). Laminated sediments are fluvial in origin and relate to subaqueous deposition in a backswamp of the formerly more extensive Khotan River. Subfossil wood associated with landform is to the upper right of the photograph. Panel B: Close view of laminated sediments.

relict shoreline at 800 m above sea level (a.s.l.) marks a former highstand of Lop Nor (Figs. 1 and 4) when it had an area of ~19,800 km^2 and a maximum depth of ~18 m.

Stands of well-preserved subfossil *Populus euphratica* and *Tamarix ramosissima* phreatophyte trees are rooted in waterlain
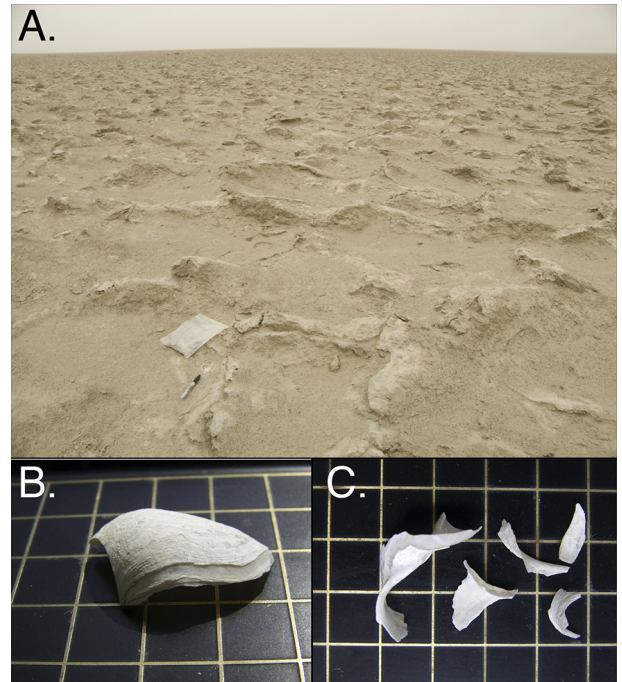
Fig. 4. Panel A: Photograph of Lop Nor lake bed, site 5 (Fig. 1). Mud-cracked lacustrine sediments contain subfossil bivalves and gastropods. Panel B: One half of a bivalve shell (LN-10-01). Panel C: Bivalve shell fragments (LN-10-02).

sediments preserved in the Taklamakan Desert. Both species are indicative of riparian forests and both require high groundwater surfaces for germination and sapling survival, as well as persistent access to groundwater for long-term growth (Gries et al., 2003). Subfossil *Phragmites* sp. [i.e., 'common reed' of Eurasian wetlands (Thevs et al., 2007)] were also found rooted in these waterlain sediments. At the Lop Desert, desiccated lakebed sediments contain bivalve and gastropod shells. Landforms in the now-dry Taklamakan Desert and paleolake shorelines in the Lop Desert, together with subfossil phreatophyte vegetation and faunal assemblages, constitute direct physical and biological evidence for higher-than-present groundwater surfaces.

We employed ^{14}C dating to determine ages of subfossil wood, reeds, and lacustrine bivalves and gastropods. In addition, targeting subfossil *P. euphratica* and *T. ramosissima* specimens with visible rings, we combined ^{14}C dating with dendrochronology to refine the timing of sapling recruitment during intervals when these trees were alive. Recruitment dates indicate times when the groundwater surface was persistently at or very close to the land surface, permitting germination and survival of sapling trees. We compiled recruitment dates based on tree-ring data collected in A.D. 1983 from living trees in regions in the northern Tarim Basin now unsuitable for sapling survival. Methods are reported in the Appendix. Whereas ages of recruitment and growth correspond to periods of sustained wetter-than-present conditions, and are thus climatically and hydrologically significant, we note that dates of tree death can relate to a number of non-climatic factors (such as disease, meandering stream channels, etc.). Therefore, in the interest of assessing implications for past hydroclimate, we discuss only chronological data that document tree recruitment and growth.

2. Geomorphology of study sites

We focused our study on five sites in the Tarim Basin (Fig. 1). Sites 1–4 in the Taklamakan Desert are associated with now-dry channels of river systems that emanated from the Kunlun and

Tien Shan drainage basins. Sites 1 and 2 (Fig. 1) are two and three km east, respectively, of a dry distributary channel of the Khotan River (Fig. 1). Site 3 is ~50 km north of where the dry northern end of the Aktash River channel is obscured by migrating sand dunes of the Taklamakan Desert. Site 4 is within a set of now-dry distributary channels of the Tarim River. The landscapes of Sites 1–4 are all characterized by wind-deflated platforms composed of finely laminated sand and silt (Figs. 2 and 3). These sediments indicate subaqueous deposition within low-flow fluvial environments (e.g., backswamps associated with floodplains of meandering river channels). The platforms of waterlain sediment are partially overlain by migrating sand dunes (Fig. 2). Rooted in the waterlain sediments of these platforms are subfossil phreatophyte *P. euphratica* (Fig. 2) and *T. ramosissima* trees, as well as *Phragmites* sp. stems and rhizomes, which indicate that the former fluvial environment featured a riparian ecosystem at Sites 1–4. Overall, we interpret the geomorphology of Sites 1–4 to record a switch from a landscape dominated by aggradation of fine-grained fluvial sediment, to the dry degradational landscape of today, which is dominated by eolian processes such as wind erosion and dune migration.

Site 5 is in the Lop Desert at ~797 m a.s.l. and ~6 km north of a 800-m a.s.l. shoreline of the southeastern sector of paleolake Lop Nor. Site 5 features a desiccated pan composed of lacustrine sediments deposited during a former highstand of paleolake Lop Nor. This site was submerged beneath three meters of water when the 800-m shoreline was constructed. The lacustrine sediments contain gastropod and bivalve shells.

3. Results

Forty-two ^{14}C dates of organic remains collected from waterlain sediments at four Taklamakan Desert sites and one Lop Desert site range in age from A.D. 1180 to A.D. 1820 (Figs. 1 and 5; Table A1). Thirty of these ^{14}C dates are on *P. euphratica* wood samples from Taklamakan Desert sites. Ten of these thirty ^{14}C dates are on wood samples from inner and outer tree rings of *P. euphratica* trees in which the intervening number of rings have been counted, thus improving dating uncertainties (Table A2). The ^{14}C chronology demonstrates the presence of living trees at least as early as A.D. 1320 until at least as late as A.D. 1820. These data indicate that the groundwater surface during this interval was persistently higher than today in now-treeless portions of the Taklamakan Desert (Fig. 2). In addition, ^{14}C dates of *T. ramosissima* (at site 2; Fig. 1) and *Phragmites* sp. (at site 3; Fig. 1) at two Taklamakan Desert sites document higher-than-present groundwater surfaces from at least as early as A.D. 1180 until at least as late as A.D. 1270. Our compilation of 250 dendrochronologically determined recruitment dates from living *P. euphratica* (Li et al., 1989) (Supplementary Table S1) reinforces conclusions obtained from ^{14}C data by indicating persistent sapling recruitment from A.D. 1674 to A.D. 1907 at sites in the northern Taklamakan Desert (Figs. 5 and 6) now too dry for *Populus* germination.

At the Lop Desert, we obtained six ^{14}C dates from a palimpsest deposit of five bivalve shells and one gastropod shell collected from desiccated lake-bed sediments (Fig. 4) at Site 5 (Figs. 1, 5 and 6). One bivalve shell affords an age of A.D. 1181 ± 58 yrs, and five other samples from the same site range in age from A.D. 1387 to A.D. 1532 (Table A1).

4. Historical Lop Nor and its desiccation

Our geomorphic and chronologic data indicate that the Tarim Basin was wetter than today beginning as early as A.D. 1180 and continuing until A.D. 1907. Historical accounts and maps reinforce this conclusion. The oldest physical description of Lop Nor (also referred to as Kara Khatun, Kara Koshun, and Kara Buran) comes from a Sogdian account called the Tarikh-i-Rashidi, written by Mirza Muhammad Haidar Dughlát between A.D. 1541–1544 (Dughlát, 1544). As described by Prejevalsky (1879; p. 26): "*In the Tarikhi Rashidi, of Mirza, Lake Lob is mentioned as covering an area four months' journey in circuit...*". In A.D. 1732, Swedish cartographer Johan Gustav Renat produced detailed maps of Central Asia and the Tarim Basin that depicted a contracted Taklamakan Desert surrounded by widespread riparian savannah, with extensive and conjoined river systems, including the Tarim River emptying into a large lake in the Lop Desert (Poppe, 1955). Renat constructed these maps using information obtained from his Dzungarian (Kalmuk, Oirat) Mongol captors. This mapped area of Lop Nor shortly prior to A.D. 1732 is consistent with our reconstruction of the lake when it stood at the shoreline about 800 m a.s.l. (Fig. 1). Historical maps and documents compiled by Yang et al. (2006) depict Lop Nor in an expanded state during the Qing Dynasty (A.D. 1644 – A.D. 1912). In A.D. 1890, Russian General M. V. Pevstoff visited Lop Nor (Kozloff, 1898) and described the lake as having an 'oval shape', a long axis of more than ~100 km from northeast to southwest, and a width of about ~40 km. Based on Pevstoff's rough dimensions, we estimate that the lake at that time occupied an area of ~3000 km^2. During his A.D. 1890 expedition, Pevstoff also interviewed a local elder in the village of Abdal (Fig. 1) named Abdul-Karim, apparently aged 110 years, who described a major contraction of Lop Nor over his lifetime. Abdal village is situated on the lower reaches of the Tarim River and lies about 13 km southwest of the 800-m paleoshoreline. Abdul-Karim described the lake during his youth in the early-to-mid A.D. 1800s as "stretching as far as the eye could see" from the village of Abdal. Abdul-Karim further recounted a progressive recession of Lop Nor from Abdal during the later part of the 19th century that forced the abandonment of many settlements in the region (Kozloff, 1898).

Observations by Prejevalsky (1879), Stein (1903), Huntington (1907), and Hedin (1940) suggested contraction of Lop Nor during the late nineteenth and early twentieth centuries, with the lake shrinking to ~10% of its former area by about A.D. 1930 (Hörner and Chen, 1935; Li et al., 2008). By A.D. 1941 Lop Nor had shrunk to a small marshland at the terminus of the Tarim/Konqi River delta (Li et al., 2008). In Fig. 6, our ^{14}C data and these historical records are summarized as a single curve that depicts changes in the area of Lop Nor over the past millennium.

5. Hydrological modeling

We conducted hydrologic modeling to identify the climate conditions necessary to sustain a closed-basin Lop Nor at the documented level of 800 m a.s.l. We combined a snow massbalance model (Birkel et al., 2012; Putnam et al., 2013), a watershed water-balance model (McCabe and Markstrom, 2007), and a lake-evaporation model (based on Priestley and Taylor, 1972) to simulate the overall steady-state hydrologic response of the lake under two derived climate scenarios: 1) the A.D. 1950s decade, shortly after the disappearance of Lop Nor, but prior to the initiation of industrialized irrigation and water-diversion practices (hereafter referred to as 'modern'); and 2) the middle 19th century, when Lop Nor stood at its 800-m level under a cooler and wetter climate relative to the A.D. 1950s.

The models were forced using gridded atmospheric temperature and precipitation datasets obtained from WorldCLIM (for temperature) (Hijmans et al., 2005) and the NASA Modern Era Retrospective Reanalysis for Research and Applications (MERRA) (Rienecker et al., 2011) reanalysis (for precipitation). Average A.D. 1950 – A.D. 2000 gridded monthly temperature data derived from
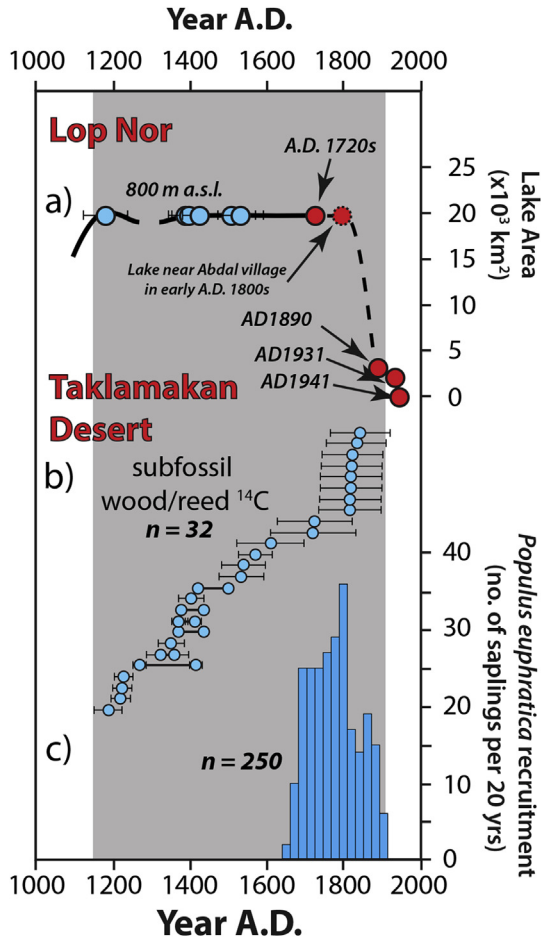
Tarim Basin
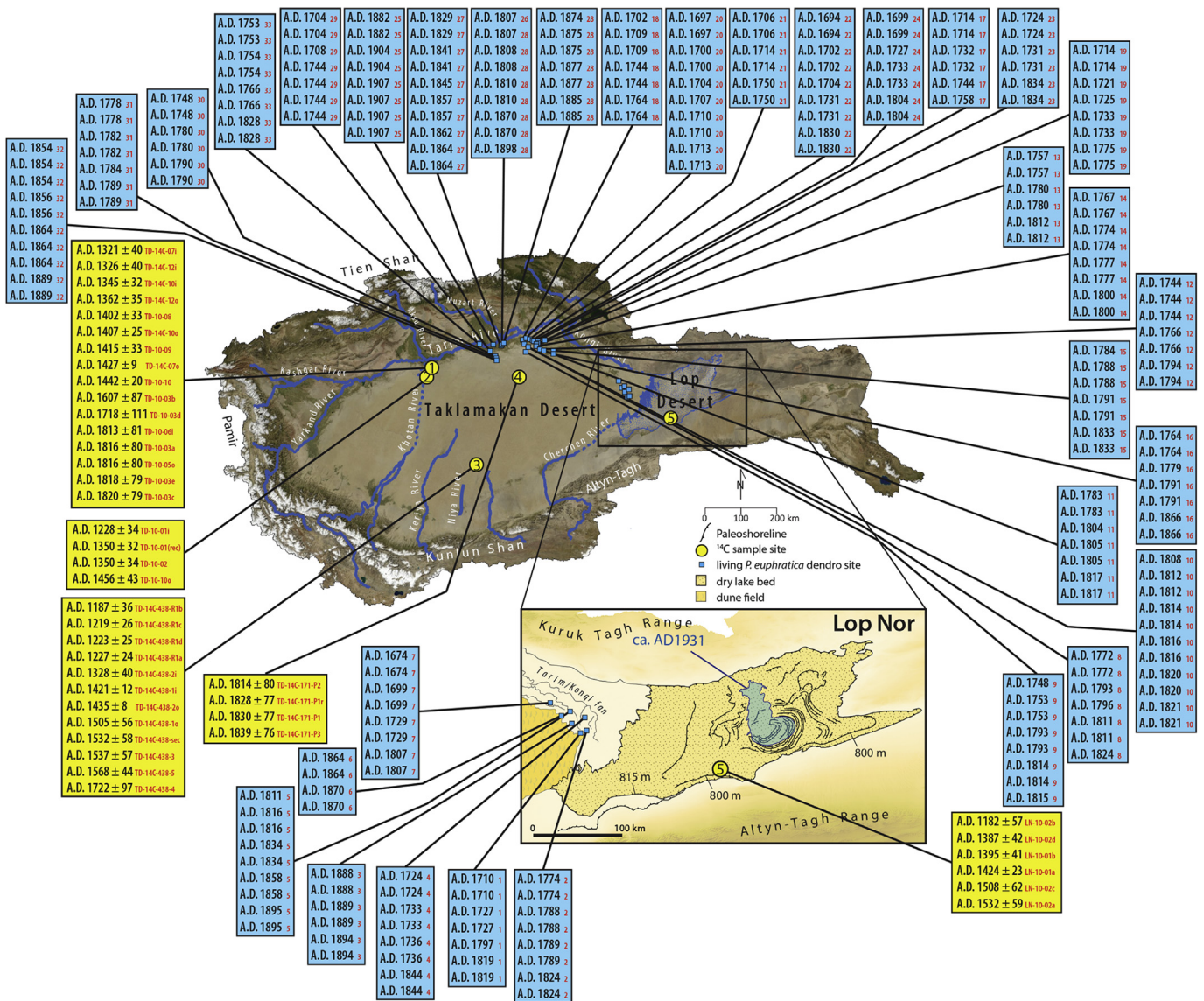
Fig. 5. Map of the Tarim Basin with chronological information displayed. ¹⁴C dates are given in yellow boxes. Red text refers to sample ID. Dendrochronological recruitment dates derived from the data of Li et al. (1989) are in blue boxes. Red text in blue boxes refers to site number given in Table S1. Map units are described in Fig. 1 legend. (For interpretation of the references to color in this figure legend, the reader is referred to the web version of this article.)

the WorldClim dataset were used as baseline input for the model. These mean annual temperature values were adjusted by ±0.7 °C and −1.6 °C to be consistent with 'modern' (i.e., A.D. 1950−1960) and middle 19th century climates, respectively. The middle 19th century simulation also accounts for the recorded decrease in seasonality since the 19th century (19th century ΔT = −4 °C relative to modern in January and −1 °C relative to modern in July).

We used gridded monthly precipitation values derived from the MERRA dataset as input to the model because this reanalysis captures orographic precipitation in mountainous regions of the Tarim Basin, such as in the Kunlun Mountains, that are not accurately represented in WorldClim. We used the average baseline MERRA precipitation grid as input for the modern scenario. For the middle 19th century scenario, we adjusted the precipitation value until a best fit was achieved between the simulated lake level and the 800-m shoreline. Our modeling approach and results are described in the Appendix and in Supplementary Table S2. The modeling results indicate that paleolake Lop Nor could have been sustained at its 800-m level with total annual precipitation values for the Tarim Basin increased by 37% above the modern value (i.e., with precipitation = 1.37 × the modern value), and with prescribed summer and winter temperatures −1 and −4 °C lower than modern values, respectively (see Appendix for details). Fig. 7 shows that, as given by the amount of runoff generated relative to the amount of precipitation at any given grid point, the area for runoff in the Tarim Basin, largely in high-mountain catchments, was larger under a climate cooler and wetter than the modern climate. Thus we conclude that Tarim Basin hydrology is sensitive to changes in high-mountain precipitation and that paleolake Lop Nor could have been sustained under a −1.6 °C mean-annual cooling and a 37% increase in total precipitation above modern values (Fig. 7).

Fig. 6. Evidence for wetter-than-present conditions in the Tarim Basin. a) Lop Nor lake-level change, based on ^{14}C dates of shells from the 800-m shoreline (blue-filled circles), and historical accounts and maps (red-filled circles; see Supplementary Information). b) ^{14}C chronology of subfossil vegetation at Taklamakan Desert sites (error bars: 1σ). Blue dots connected by horizontal black lines: dendrochronological tree-growth intervals. c) *P. euphratica* sapling recruitment over 20-yr intervals. Vertical grey band: duration of wetter-than-present conditions in the Tarim Basin. (For interpretation of the references to color in this figure legend, the reader is referred to the web version of this article.)

6. Discussion

6.1. Tarim Basin hydroclimate and the Little Ice Age

The timing of the rise of the groundwater surface in the Tarim Basin, as provided by our reconstruction, suggests a wetter-than-present climate in the Tarim Basin and across much of the Asian mid-latitude desert belt. In the Tarim Basin, our chronology is compatible with, and augments, proxy reconstructions for local humidity, inferred from the δ^{13}C of *Tamarix* sp. leaf matter (Liu et al., 2010) and lacustrine sediment proxies (Chen et al., 2006a) at sites in the northern Tarim Basin. Our record is also compatible with historical evidence for increased runoff in the Keriya River during the Little Ice Age (Yang, 1991; Yang et al., 2006). On a broader scale, our record matches chronologies of wetter-than-present conditions elsewhere in Eurasian middle latitudes from the late A.D. 1100s until the A.D. 1800s. For example, rises in the levels of the Dead Sea (Enzel et al., 2003), the Caspian Sea (Haghani et al., 2015), and groundwater-fed lakes on the Swiss Plateau (Holzhauser et al., 2005) were all broadly contemporaneous with the rise of the Tarim Basin groundwater-surface elevation as documented here.

Responding to atmospheric cooling and snowline lowering, Northern Hemisphere mountain glaciers expanded to late-Holocene 'Little Ice Age' extents (Denton and Karlén, 1973; Luckman, 2000; Grove, 2001; Holzhauser et al., 2005; Denton and Broecker, 2008) coeval with wetting of the Tarim Basin. Precisely dated records of glacier fluctuations in the European Alps (Grove, 2001; Nicolussi and Patzelt, 2001; Holzhauser et al., 2005), British Columbia (Ryder and Thompson, 1986; Luckman, 2000; Mood and Smith, 2015), and Alaska (Barclay et al., 2009, 2013), based on dendrochronological and ^{14}C analyses of glacially sheared subfossil tree-stumps rooted in glacier forelands, indicate that northern mid-latitude glaciers first expanded and reached close to Little Ice Age maximum positions between A.D. 1142 and A.D. 1350 (Fig. 8). Outlet glaciers of small ice caps in east Greenland had also achieved Little Ice Age positions by about A.D. 1180 (Lowell et al., 2013). This phase of glacier expansion in western North America is known as the "early" Little Ice Age (Luckman, 2000; Barclay et al., 2009). Subsequent glacier advances to Little Ice Age maxima in the Swiss Alps culminated at A.D. 1600–1667 and A.D. 1859, and in western North America by about A.D. 1725 and A.D. 1850 (Luckman, 2000; Denton and Broecker, 2008; Barclay et al., 2009, 2013). The last advance of boreal mid-latitude glaciers that culminated in the A.D. 1850s was followed by recession that marked the end of the Little Ice Age, and has continued, with minor fluctuations, until the present day.

To explain coeval expansion of northern glaciers and rise of the Tarim groundwater surface, we suggest that at the beginning of the early Little Ice Age in the late A.D. 1100s, wintertime spread of North Atlantic sea-ice (Lamb, 1979; Denton and Broecker, 2008; Nagashima et al., 2011; Pausata et al., 2011) (Fig. 8) and cooling of the downstream Eurasian continent strengthened and/or shifted the mean position of the westerly jet south of its present-day position. Thus the jet would have maintained a stronger and more persistent summertime alignment with the circum-Tarim mountain ranges, akin to the present-day springtime circulation in the region (Nagashima et al., 2011), thereby stimulating expansion of mountain glaciers and winter snowpack, as well as intensified orographic precipitation. By this hypothesis, a combination of glacier/snowpack expansion (Berghuijs et al., 2014) and intensified orographic precipitation (Nagashima et al., 2011; Dettinger, 2014; Luce et al., 2014) increased mountain runoff and hence stimulated the rise of mid-latitude Eurasian water tables. A strengthened and southward-displaced jet would also have suppressed the seasonal development of the south Asian monsoon systems (Chiang et al., 2015), leading to an anti-phased hydroclimatic response to Little Ice Age cooling between interior and monsoonal Asia. This hypothesis is supported by evidence for Little Ice Age weakening of Asian monsoon coeval with wetting of the Taklamakan and Lop Deserts.

6.2. Early Little Ice Age wetting of interior Asian deserts and expansion of the Mongol Empire

The onset of wetter-than-present conditions in Asian deserts during the Little Ice Age may have stimulated the formation of the greatest land empire ever on Earth. Here we suggest that southward expansion of steppe grasslands in response to elevated groundwater surfaces aided the spread of the Mongols, led by Chinggis Khan, out of the Mongolian heartland and across the Asian arid belt after A.D. 1206 (Fig. 8; Table A3). Thus the Mongol rise may be tied to the atmospheric conditions associated with the onset of Little Ice Age cooling.

The concept that climate change was somehow involved with the episodic spread of pastoralists from their Eurasian steppe homelands can be traced back at least a century. Huntington (1907)

Runoff Coefficient
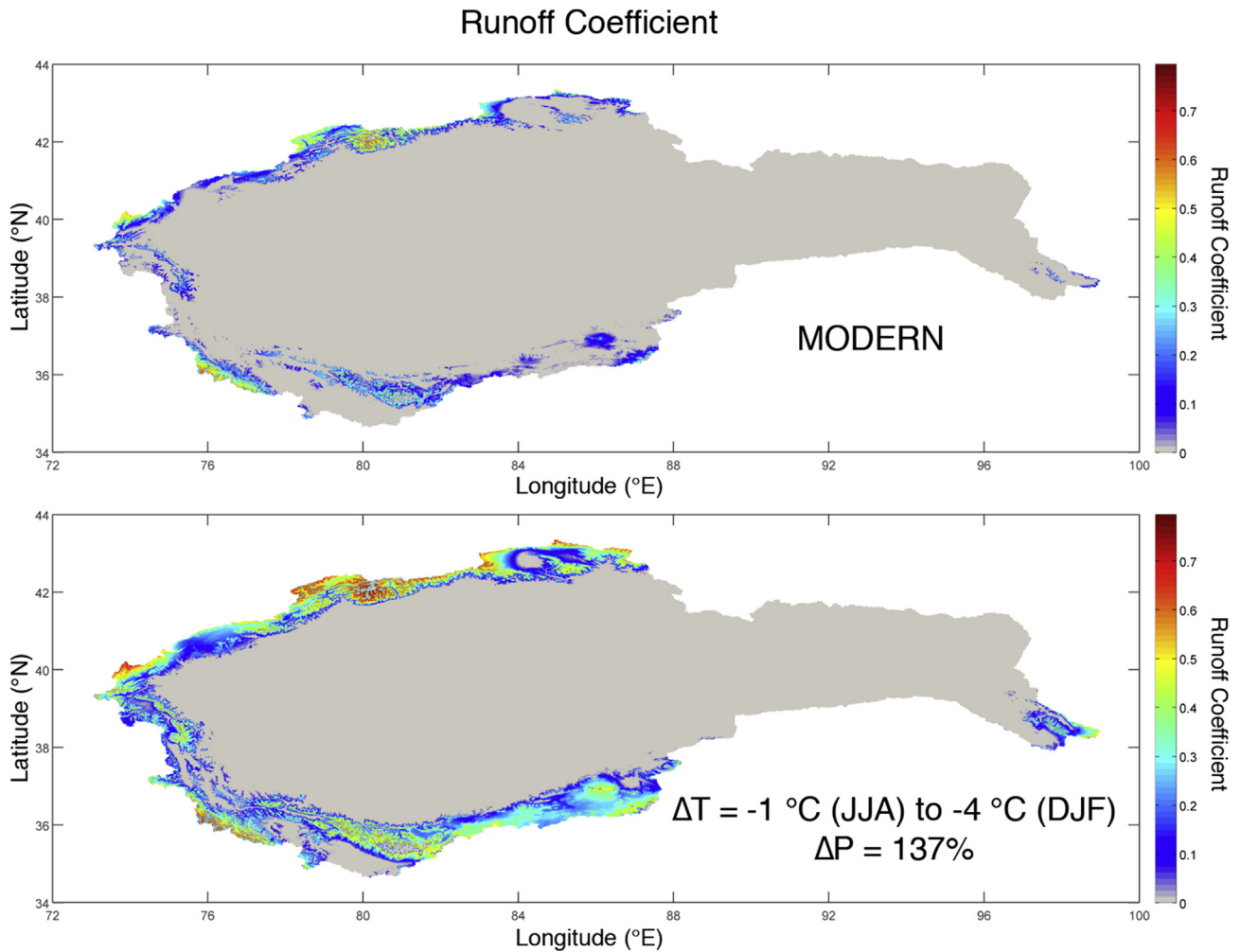
Fig. 7. Maps showing Tarim Basin runoff coefficient (color scales). Top panel: Runoff coefficient values corresponding to the modern (control) simulation. Bottom panel: Runoff coefficient values for the scenario in which Lop Nor is sustained at the 800-m lake level. (For interpretation of the references to color in this figure legend, the reader is referred to the web version of this article.)

proposed a "pulse" of nomadic and sedentary states across the ecological and geographic divide between the steppe and China. In a note published and illustrated in Tonybee (1934), G.F. Hudson suggested that Mongol expansion followed climate-driven latitudinal shifts of boreal forest, steppe, and desert biomes. Tonybee (1934) and Lattimore (1938) pointed to the "weaknesses of the climatic theory, when taken unmodified and accepted as all-explanatory" (Tonybee, 1934, pp. 453–454). Jenkins (1974) later noted that periods of glacier advance in Europe were coeval with nomadic irruptions out of the Mongolian steppe, and on that basis proposed a link between nomadic irruptions and climatic cooling. More recently, Pederson et al. (2014) attributed the Mongol rise to a fifteen-year-long episode of wet conditions in the Mongolian heartland, based on climatic interpretations of tree-ring sequences in Mongolia.

We suggest three ways in which the wetting of interior Asian deserts at the onset of the Little Ice Age may have contributed to the rise of the Mongol Empire. First, wetter conditions leading to increased biomass in arid regions could have fueled the military conquests of Mongol horsemen across Eurasia (Fitzhugh, 2013; Pederson et al., 2014). The timing of the Mongol expansion, beginning with the first campaign against the Tanguts of Xi Xia in A.D. 1207 and the annexation of the Uyghur and Qarluk Türks in A.D. 1209 (Curtin, 1908), corresponds with the timing of increased

runoff and groundwater-surface rise in the arid belt south of Mongolia, as recorded in the Tarim Basin (Fig. 8). Mongol Empire cavalry soldiers typically took three or more remounts on campaign. Thus an army of 20,000 horse soldiers would include more than 60,000 horses (Rossabi, 1994). Grass was the energy source that fueled the horse-driven military conquests of the Mongol Empire — an early *blitzkrieg* with horses rather than panzers (Fitzhugh, 2013). Because Mongol horses were expected to forage during long-ranging military campaigns, and therefore could not rely solely on fodder from the grasslands of the Mongolian steppe, the greening of mid-latitude Asian deserts may have been a key factor permitting transit of Mongol cavalry to regions distal to the Mongolian heartland.

Second, the "pull" southward of expanded grasslands, together with a "push" southward by harsh winters, may have provided double incentive for Mongol steppe pastoralists to migrate southward. The Türkic-, Mongol-, and Tungusic-speaking pastoralists of the steppe were dependent upon the carrying capacity of rangeland. Hudson (in Tonybee, 1934) suggested that the link between climate and cultural migrations across the steppe related to the subsistence strategy of steppe pastoralists. This strategy involves pastoral herders' use of "the five snouts" (*tavan khoshuu mal*): (1) horses, (2) cattle/yaks, (3) camels, (4) sheep, and (5) goats (e.g., Barzagur, 2002). The five snouts are listed in the order of their
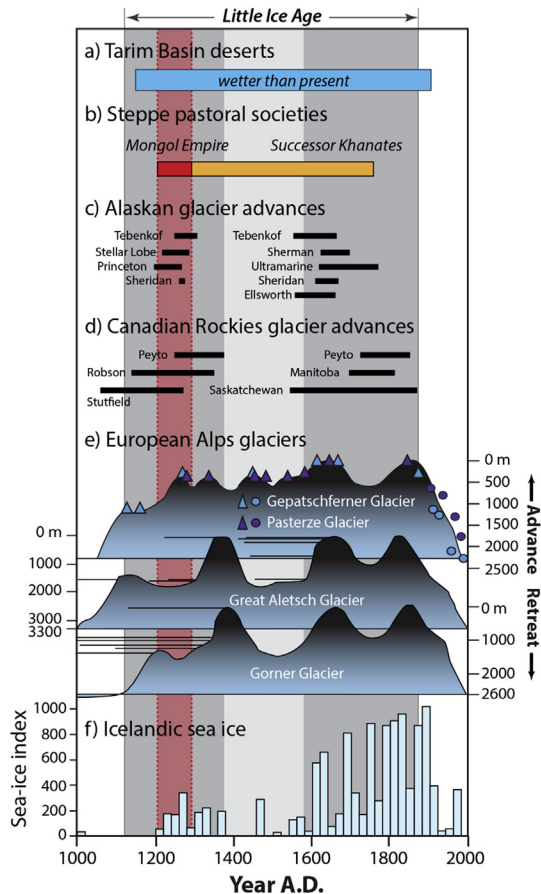
Fig. 8. Wetter-than-present conditions in the Tarim Basin (blue bar, panel a) compared with records mentioned in text. b) Timeline of Mongol Empire (red) and Khanate successors (orange), based on information in Table A3 c–e) Northern Hemispheric glacier fluctuations. Thick black bars in c) and d) represent phases of glacier advance. Colored triangles: dendrochronological and ^{14}C ages of Austrian glacier advances. Colored circles: historical glacier positions. f) Sea ice off the north coast of Iceland (Lamb, 1979; Denton and Broecker, 2008). Index reflects duration in weeks of sea-ice occurrence along a number of coastal segments. Vertical grey bands: early and late phases of the Little Ice Age (Luckman, 2000). Vertical red band: duration of the Mongol Empire from A.D. 1206 until A.D. 1294 (Table A3). (For interpretation of the references to color in this figure legend, the reader is referred to the web version of this article.)

relative cultural value (Atwood, 2004; Bosson, 2013). We add to this list a sixth "snout", reindeer, to include the boreal taiga north of the Eurasian steppe. This modified "six snout" concept illustrates the efficient conversion of all types of rangeland from boreal taiga to sand desert (including grassland, mountain scrub, alpine meadows, and desert scrub) into energy (meat, milk, dung, and transportation) and commodities (hides, hair, horn, and sinew).

A southward shift of interior Asian ecological zones would have required adaptation by pastoral herders. Winter range for livestock is perhaps the most important factor governing the carrying capacity of herds not provided with harvested fodder in winter. Today, steppe pastoralists have 20 to 50 animals per person (Atwood, 2004). Thus a group of 100 herders must find pasture for at least 2000 animals. Any change in the quality of winter grazing has immediate impacts on herds and herders. We suggest that cold winters and prolonged snow and ice cover on the steppe at the onset of the Little Ice Age may have resulted in a net southward shift of optimum winter rangeland for each of the six snouts, perhaps providing additional incentive for steppe pastoralists to migrate south.

Third, greening of the desert may have sparked a shift from agriculture to pastoralism among desert oasis dwellers (Lattimore,

1938). The settled societies in the mid-latitude drylands, including the Uyghurs, Qara-khitans, and Qarluq Türks, practiced oasis irrigation agriculture. The deleterious impacts on agriculture of shorter growing seasons and late frosts attending the onset of the Little Ice Age may have outweighed the benefits of increased precipitation and runoff. At the same time, the South Asian Empires, subsisting on rice agriculture, were experiencing drought, famine, civil unrest, and rebellion on account of weakened monsoon rainfall (Zhang et al., 2008; Buckley et al., 2010). Thus southward expansion of grazing land may have helped stimulate a shift toward pastoral nomadism among central Asian agriculturalists, thereby strengthening their economic and cultural ties to the Mongols.

In summary, the spread of the Mongol Empire from A.D. 1206 to A.D. 1241 was coeval with the early phase of Little Ice Age glacier expansion in northern middle latitudes (Ryder and Thompson, 1986; Luckman, 2000; Nicolussi and Patzelt, 2001; Holzhauser et al., 2005; Barclay et al., 2009, 2013; Mood and Smith, 2015). We propose here that impacts of Little Ice Age climate dynamics on the water balance of interior Asia stimulated southward spread of grazing land that helped fuel Mongol conquests across Eurasia. Sustained wetter-than-present Little Ice Age conditions in the desert belt would have favored persistence of widespread pastoral societies for centuries, even well after the gradual geopolitical disintegration of the Mongol Empire.

6.3. Impacts of future warming on interior Asian hydrology

In contrast to wetter-than-present conditions that attended the Little Ice Age and that may have aided the spread of the Mongol Empire across Eurasia, drying since the late 19th century has led to overall diminution of water across much of the Asian desert belt. Lowering of the Tarim Basin water table over the past century has accompanied climatic warming. On the basis of our reconstruction, we consider that the duration and magnitude of the current Tarim Basin drought is exceptional within the context of the past ~830 yrs. As atmospheric CO_2 concentrations increase, warming of the continent-rich Northern Hemisphere is expected to outpace warming in the ocean-rich Southern Hemisphere (Chiang and Friedman, 2012; Broecker and Putnam, 2013; McKinnon and Huybers, 2014). Steepening of the interhemispheric temperature gradient may stimulate a northward shift of Earth's thermal equator, along with weakening and/or northward movement of the boreal westerlies (Chiang and Friedman, 2012; Broecker and Putnam, 2013). Continued CO_2-driven radiative heating of the Eurasian land surface (McKinnon and Huybers, 2014), together with slackening and/or northward migration of the westerly jet (Xu and Ramanathan, 2012; Broecker and Putnam, 2013; Friedman et al., 2013; Dettinger, 2014; Luce et al., 2014; Chiang et al., 2015), could spur drought intensification and northward expansion of mid-latitude Asian deserts. Increasing scarcity of available water in these regions could have destabilizing socioeconomic impacts, and therefore should be considered in regional management policies.

7. Conclusions

1) A ^{14}C chronology of subfossil trees and reeds associated with waterlain sediments at four sites in the Taklamakan Desert, as well as mollusks associated with an elevated shoreline documenting the presence of the ~19,800 km^2 closed-basin lake Lop Nor, indicates that the Tarim Basin was continuously wetter than today at least as early as A.D. 1180 until the middle A.D. 1800s. This chronology is reinforced by 250 dendrochronologically constrained *P. euphratica* recruitment ages from living trees showing that the northern reaches of the Taklamakan Desert were sufficiently wet to support sapling survival and tree

growth between A.D. 1674 and A.D. 1907. Our chronologies dovetail with historical accounts and maps documenting a contracted Taklamakan Desert and an expanded Lop Nor in the A.D. 1730s and middle A.D. 1800s, as well as a subsequent decline of Lop Nor surface levels in the latter A.D. 1800s and into the A.D. 1900s.

2) The results of a hydrological modeling exercise, which included integration of a snow mass-balance model, a watershed-balance model, and a lake-evaporation model, suggest that a climate colder and at least 37% wetter than today could have supported Lop Nor at its 800-m level. Because of difficulties accounting for water losses in transport to Lop Nor (e.g., due to evaporation), we cannot rule out the possibility that the Tarim Basin was even wetter than suggested by this analysis. Thus our result may be a minimum estimate for the amount of precipitation decrease since the middle 19th century.

3) Our chronology accords with other paleohydrological records from Eurasian middle latitudes and is coeval with the timing of well-documented circum-Northern Hemispheric mountain glacier expansions that define the Little Ice Age period (ca. A.D. 1150 to A.D. 1845). We attribute Little Ice Age wetting of the Tarim Basin deserts to a strengthening and/or southward shift of the boreal westerlies, resulting in an expansion of mountain snowpacks and an invigoration of orographic precipitation in the high mountains forming the rim of the Tarim Basin.

4) The onset of wetter-than-present conditions in the Tarim Basin coincided with the Mongol expansion, under the leadership of Chinggis Khan, across the mid-latitude Asian deserts that established the largest contiguous land empire ever known. We propose that wetting of the interior Asian desert corridor stimulated southward migration of winter rangeland, which was essential in fueling the horse-driven Mongol conquests across Eurasian deserts. In addition, wetter-than-present Asian deserts may have aided in the spread of pastoralism out of the Mongolian heartland, strengthening cultural and economic affinities among the Mongols and Türkic-speaking groups on the periphery of the steppe.

5) Warming of interior Asia since the end of the Little Ice Age and throughout the 20th century led to a net drying of the Tarim Basin. Ongoing warming could lead to further weakening and/or northward migration of the boreal westerlies, which in turn could cause Asian deserts to expand northward.

Appendix B. Supplementary data

Supplementary data related to this article can be found at http://dx.doi.org/10.1016/j.quascirev.2015.10.033.

Appendix A

A.1. Chronology

A.1.1. ^{14}C dating

Samples collected for ^{14}C dating were transported to the Lamont-Doherty Earth Observatory and prepared for ^{14}C analyses. We cleaned wood, reed, and shell samples of any foreign sedimentary or organic matter. In cases noted in Table A1, we sub-sampled individual tree rings under a microscope using a scalpel. ^{14}C pretreatments and Accelerator Mass Spectrometry (AMS) measurements were conducted at the Swiss Federal Institute of Technology Zürich (ETH), as well as at the University of California, Irvine, W.M. Keck Carbon Cycle AMS Laboratory (UCI-AMS). We converted ^{14}C age determinations to calendar ages using the OxCal 4.2 program (Bronk Ramsay, 2009; Bronk Ramsay, 2011), available online (https://c14.arch.ox.ac.uk/oxcal.html), together with the IntCal13 ^{14}C calibration dataset (Reimer et al., 2013). All calendar-year converted ^{14}C dates are shown plotted in Figs. 5 and 6. The D-Sequence component of the OxCal 4.2 software was used to refine ^{14}C ages of inner and outer rings of subfossil wood samples for which the number of intervening rings had been counted (Table A2, see also Section A.1.2., below). We made no corrections for ^{14}C reservoir effects. Because of the shallow depths of Lop Nor, we assume that the water column was well mixed and that ^{14}C content of lake water was in equilibrium with the atmosphere. However, applying such a reservoir correction would result in younger ages, which would not change the result that the Lop Nor stood near the 800 m a.s.l. shoreline during Little Ice Age time.

A.1.2. Dendrochronology

Subfossil wood samples were collected from well-preserved dead standing trees ("snags") of *P. euphratica* (four and two individuals at sites 1 and 3, respectively) and *T. ramosissima* (two individuals at site 2). Cross-sections were sanded until cells were visible under a microscope. Samples were processed and rings were counted following standard dendrochronological procedures (Cook and Kairiukstis, 1990) at the Lamont-Doherty Earth Observatory Tree-Ring Laboratory. Ring counting provides the number of years between the inner ring (next to the pith) and the outermost preserved ring. Considering that ^{14}C ages from the past millennium often yield multiple calendar-age solutions because of complexity in the chronology of atmospheric ^{14}C activity, tree-ring analyses were instrumental in improving calendar-year-converted ^{14}C-age uncertainties (Table A2).

Here, we do not claim exact calendar dates of tree recruitment because the first ring formed is uniquely located at the base of the tree and most samples were collected at ~1–1.5 m above the base. However, we assume that the innermost rings dated here probably represent the period of recruitment to about a decade or so — the data are depicted in 20-yr bins in Fig. 6. In addition, abrasion by blowing sand has scoured the outer wood of many of the subfossil trees sampled here. Therefore, we do not assume that the outermost ring of each individual tree necessarily represents the age of death.

Recruitment dates of living *P. euphratica*, compiled in Figs. 5 and 6 and Table S1, were derived from tree-ring data collected in A.D. 1983 from 250 living trees at Bayinguoleng (40.28°N; 88.21°E), Donghetan (40.94°N; 84.86°E), Luntai (41.33°N; 84.68°E), and Aksu (40.91°N; 83.36°E), and processed by the Xinjiang Laboratory of Tree-Ring Ecology of the Institute of Desert Meteorology (Li et al., 1989).

A.2. Hydrological modeling

A.2.1. Overview

To identify climatic conditions that would have sustained paleolake Lop Nor at its 800-m level, we combined a snow/ice mass balance model with a watershed balance model and a lake evaporation model. Here we describe our modeling framework. First, we employed a snow/ice mass balance model, forced with input from gridded climatological data obtained from WorldClim and MERRA, to produce gridded fields of monthly temperature, rainfall, and snowmelt. These fields were, in turn, used as input for a lake evaporation model, which generated estimates of Lop Nor water balance. Finally, we used a watershed balance model with gridded climate data as inputs, to determine the total amount of runoff reaching the Lop Nor basin. With this model framework in place, we conducted two simulations: 1) a 'modern' simulation utilizing climate parameters of the A.D. 1950 − A.D. 1960 decade, i.e. shortly before the onset of industrialized irrigation in the Tarim Basin; and 2) a middle 19th century (i.e., Little Ice Age) simulation, in which atmospheric temperature was prescribed using values extrapolated from late-19th century instrumental temperature data, and in which basin-wide precipitation values were adjusted until the modeled level of Lop Nor matched the 800-m shorelines formed during the Little Ice Age.

A.2.2. Selection of model domain and climate data input

We utilized a 3-arc-second (90-m) resolution digital elevation model (DEM) for the Tarim Basin using NASA Shuttle Radar Topographic Mission (SRTM) data. We used this DEM to identify and delineate important topographic features in the Tarim Basin, such as the Lop Nor 800 m lake level and the corresponding contributing watershed area.

To set the stage for hydrological modeling, we developed a modeling grid with estimates of elevation, latitude, and climate (i.e., values of monthly precipitation and temperature) provided for each grid cell. We selected a 30 arc-second (~1 km) rectangular domain (3112 columns by 1047 rows) in a tight crop around the entire Tarim Basin. Each of the 3,258,264 grid cells in the domain was identified either as a lake cell (corresponding to the 800 m Lop Nor), a watershed cell (area contributing runoff to the 800 m Lop Nor), or as an inactive cell (outside the watershed boundary).

Baseline temperature for the A.D. 1950 − A.D. 1960 control run was defined from WorldClim (Hijmans et al., 2005), which is a gridded monthly global climate data set (spanning the period from A.D. 1950 to A.D. 2000) that incorporates a thin-plate smoothing spline method to register interpolated values of scattered meteorological station data onto a continuous 30 arc-second SRTM DEM. We applied a +0.7 °C correction relative to the A.D. 1950−2000 mean [derived from NCEP/NCAR Reanalysis (Kalnay et al., 1996)] to the WorldClim grids in order to match the A.D. 1950−1960 climate.

Although the WorldClim data set includes precipitation estimates, we elected to use an alternative data set for precipitation input after initial testing revealed significant rainfall deficits across mountainous areas that have sparse or no station data coverage (Fig. A1). In contrast to temperature, which can be interpolated accurately between distant points over complex terrain using standard atmospheric lapse rates, precipitation develops from nonlinear processes (e.g., convection and orographic uplift) and cannot be scaled in a meaningful way without dense data control. Thus we used the monthly-averaged gridded precipitation data (A.D. 1979−2000) from the NASA MERRA (Rienecker et al., 2011) framework. MERRA is a state-of-the-art dynamical reanalysis model that produces weather between 6-hourly ingests of meteorological observations (station, radiosonde, and satellite). The reanalysis captures orographic precipitation across remote parts of

the Tarim Basin that are not represented in WorldClim (Fig. A2). While MERRA affords a reasonable representation of precipitation across the Tarim Basin, we note caveats, including the relatively coarse nominal grid resolution of 0.5° × 0.667° (fit to the 30 arc-second Tarim model domain using bilinear interpolation), and limited time period that spans only the latter half of the WorldClim data set.

Climate input fields for the middle 19th century scenario were made by applying temperature and precipitation anomalies [ΔT (°C) and ΔP (%)] to our combined WorldClim-MERRA climatology. Temperature anomaly values are based on meteorological data from Tashkent, Uzbekistan, ~600 km east of the Tarim Basin (Fig. A3). Although Tashkent is outside of the Tarim Basin, the observed temperature record from this station spans a longer interval than any other set of meteorological observations in the region, with nearly continuous temperature measurements beginning ca. A.D. 1890 [see also Solomina et al. (2004)]. Because Tashkent is upwind of the Tarim Basin, and because temperature trends are broadly correlated across interior Asia (Davi et al., 2015), we consider that the temperature record from this area affords a reasonable approximation for the temperatures over the Tarim Basin.

We defined the middle 19th century scenario using conservative seasonal anomaly estimates: ΔT = −4 °C Jan to −1 °C Jul (mean annual ΔT = ~−1.6 °C). We note that choosing a slightly cooler temperature value, (e.g., mean annual ΔT = −2.0 °C), does not significantly alter the results of this study.

Because precipitation data are absent in the Tarim Basin for the 19th century, particularly for the mountain environments where most runoff is generated, we used our model to estimate past precipitation by incrementally adjusting ΔP (described below).

A.2.3. Modeling approach

The modern and middle 19th century simulations were conducted by running, in this sequence, the snow mass balance model, watershed water balance mode, and lake evaporation model (see Fig. A4). Each model was run separately. We ran each model until a steady state condition was achieved for the modern (dry Lop Nor) and middle 19th century (Lop Nor at 800 m a.s.l.).

Step 1: Snow Mass Balance. We calculated monthly rainfall, snowmelt, and runoff using a degree-day snow/ice mass balance model adapted from Birkel et al. (2012) and Putnam et al. (2013). Model input included monthly mean temperature and precipitation grids (here we used the composite WorldClim-MERRA climatology described above). From this input, surface mass balance was calculated by determining annual snow accumulation from the sum of precipitation for all months when temperature $T_{month} \leq 0$ °C. The model then calculated total annual ablation by summing melting degrees (md) ($md_{month} = T_{month}$ * number of days in month) for all months when $T_{month} > 0$ °C, and then reducing accumulated snow at a prescribed snowmelt rate (mm/md). If melting degrees remained once all winter snow was ablated, ice was in turn melted at an ice-melt rate. Net annual mass balance was determined by subtracting total accumulation from total ablation. In the absence of published melt factors for the Tarim region, we used typical values of 3 and 8 mm/md for snow and ice, respectively [e.g., (Braithwaite and Olesen, 1989)]. The amount of runoff due to snow and ice melt was estimated for each month as the sum of snow and ice ablation for each grid cell. The amount of runoff resulting from rainfall was estimated from the accumulation of rainfall at each grid cell.

Step 2: Watershed Water Balance. We employed a watershed water balance model based on the Thornthwaite hydrological model (Thornthwaite, 1948; McCabe and Markstrom, 2007). This water balance model has been employed extensively in studies of water-resource management and climate change (Alley, 1984;

Wolock et al., 1993; Wolock and McCabe, 1999; Legates and McCabe, 2005). We implemented our version of the Thornthwaite model in Matlab based on algorithms presented by McCabe and Markstrom (2007). This method simulates the basic components of the hydrologic cycle (soil-water storage, evapotranspiration, and runoff) for each watershed grid cell using input from climate data and the amount of liquid water available at the land surface. We used output from the snow/ice mass balance model (described above) as input for the watershed balance model. Three of the four model parameters were set to default values for each watershed grid cell (McCabe and Markstrom, 2007): fraction of direct runoff from impervious surfaces (*drofrac* = 0.0), rate of runoff from surplus storage (*rfactor* = 0.5), and soil-moisture storage capacity (*stc* = 150 mm). The fourth model parameter, the Hamon Equation Coefficient (*hamonCoef*), directly controls the amount of potential evapotranspiration (PET) and indirectly controls soil moisture storage, evapotranspiration (AET), and surface runoff (Q). The *hamonCoef* has a default value of 0.55 based on studies by Hamon (1961) for areas in the humid southeastern United States. However, Barth (2013) and McCabe et al. (2015) found that *hamonCoef* values between 0.2 and 1.8 are required order to produce reasonable PET estimates in the arid interior of the United States Great Basin, which has an arid climate similar to that of the Tarim Basin. In the absence of published *hamonCoef* values for the Tarim Basin, we identified this parameter value to be 1.4 through a manual calibration process that involved fitting basin-wide PET, estimated by the model, to estimates of PET from the Consortium for Spatial Information (CGIAR) Global Aridity and PET Database (Zomer et al., 2007, 2008).

Step 3: Lake Evaporation. To estimate the free-water evaporation from Lop Nor, we implemented a lake-evaporation model forced with monthly temperature values determined from the WorldClim and MERRA climate data. Our model was based on the Priestley–Taylor equation (Priestley and Taylor, 1972) that relates evaporation to the latent heat of evaporation and heat flux in a water body [Eq. (A.1)] (Winter et al., 1995):

$$E = \alpha \left[\frac{s}{s + \gamma} \right] \left[\frac{Q_n - Q_x}{L} \right] \tag{A.1}$$

where, E is the free-water lake evaporation (mm day^{-1}), α is the constant derived empirically by Priestley and Taylor (1972) (dimensionless), $s/(s + \gamma)$ is derived from the slope of saturated vapor pressure at the mean air temperature, γ is the psychrometric constant (dimensionless), Q_n is the net radiation (in calories per square centimeter per day), Q_x is the change in heat stored in the water body (cal cm^{-2} d^{-1}), and L is the latent heat of vaporization (cal g^{-1}). We used a value of 1.4 for the α coefficient, based on the suggestions of Jensen et al. (1990) for arid and semi-arid environments. We assumed that the impacts of lake-heat storage would be minimal (i.e, $Q_x = 0.0$) in our steady state scenarios. Values for the remainder of the parameters were selected using accepted guidelines for calculating radiation and evaporation (Allen et al., 1998).

We employed the three models to simulate a complete water balance of the Tarim Basin for the modern climate scenario by the following approach:

1. The snow-mass-balance model was run to estimate the spatial extent of seasonal snow accumulation and the total amount of liquid water available at the land surface for each grid cell in the model domain.
2. The watershed-water-balance model was run with input from the snow-mass-balance model results, as well with gridded climate data, to estimate the total runoff from each watershed grid cell in the basin.

Because Lop Nor had dried completely by the A.D. 1950s, we did not use the lake model in the modern simulation. In the modern scenario, we assume that all runoff generated does not make it to the lake due to transportation losses related to evaporation, transpiration, and/or recharge to the groundwater system. This loss, 9.84 km^3, is considered to be a minimum amount of runoff that must be overcome to transport water to Lop Nor in the middle 19th century scenario (Table S2). The runoff actually required could be much more than this amount. We consider that excess water generated by the hydrologic model under the modern scenario could reflect a combination of deficiencies related to our approach of applying a simple hydrological model to a large, complex basin with several contributing areas separated by a deep sand desert. Atmospheric recycling of moisture across the basin (Blard et al., 2011) could also provide a feedback that is not represented in our modeling approach. Finally, our approach could be substantially underestimating reduction in wind-driven orographic mountain precipitation over the past century in Northern Hemisphere middle latitudes (Dettinger, 2014; Luce et al., 2014). Additional quantification of this loss factor is beyond the scope of the simple water balance modeling approach presented here (i.e., a more detailed representation of the groundwater and surface water systems is needed), and will be the subject of further investigation.

To simulate the middle 19th century climate, we employed the three models described above. We followed the same two steps as described for the modern simulation, but added two additional steps:

3. The lake evaporation model was forced with temperature data to estimate the total evaporation from each lake grid cell for Lop Nor at the appropriate lake elevation (i.e., 800 m a.s.l.).
4. A simple summation of the basin water balance was performed to check that steady-state conditions were achieved (i.e., P + Q − E − 9.84 km^3 = 0). If steady-state conditions were not achieved, we adjusted the amount of precipitation and repeated steps 1–4 until a steady state water balance was achieved.
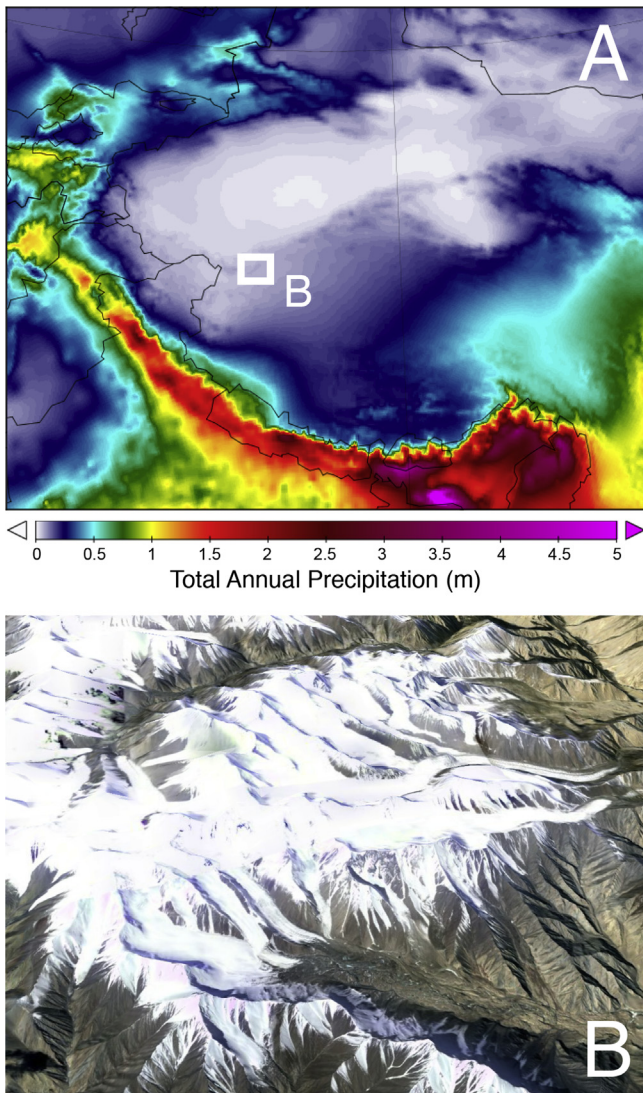
A.2.4. Model results and discussion

The results for all climate scenarios are presented in Table S2. We found that Lop Nor achieved a steady state water balance in the 19th century simulation when forced with total annual precipitation 1.37 times the modern value. In this scenario, watershed runoff (38.23 km^3) and precipitation directly onto the lake (0.40 km^3) contributed water to Lop Nor, whereas evaporation over the lake (28.21 km^3) and the minimum loss factor found from the modern run (9.84 km^3) removed water. The remaining water volume (0.59 km^3) is small compared to the magnitude of the rest of the terms; thus we consider that the result reasonably approximates the steady state water balance of Lop Nor when it stood at its 800-m level.

In each scenario, we observed that the spatial distribution of total annual runoff tends to be restricted to the mountainous topography near the edges of the Tarim Basin. Little to no runoff was generated in the lowland areas as shown in Fig. 7. There is an increase in total depth and spatial extent of annual mountain runoff under the middle 19th century conditions compared to modern conditions. We computed the basin-scale runoff ratio (total basin runoff/total basin precipitation) from the water balance information in Table S2 for the modern (0.05) and for the middle 19th century (0.15) scenarios. Although these ratios do not reflect the amount of spatial variability throughout the Tarim Basin, they do show that a 37% increase in total basin precipitation above modern values resulted in a 389% increase in total basin runoff for the middle 19th century compared with the modern scenario.

For most lowland areas of the Tarim Basin, the total amount of annual precipitation is below a threshold amount needed to generate any runoff, and the runoff coefficient is very close to zero. In other areas of the basin, the ratio of runoff per unit of additional precipitation (i.e., the runoff ratio) increases toward a maximum value of 1.0 as the amount of total annual precipitation increases above the threshold amount required for generating runoff.

We note that utilization of mountain runoff for irrigation agriculture in the Tarim Basin has intensified since the A.D. 1960s under current Chinese development programs (Thevs, 2011). These activities increase water loss through evaporation and are a contributing factor to general desiccation. A study by Hongfei et al. (2000) reported that between 70% and 99% of all water consumed in the Tarim Basin is for agricultural irrigation. For example, in A.D. 1998 irrigation agriculture used ~26 km^3 of water runoff. However, pre-industrial impacts of human water extraction were probably minor and superimposed on natural fluctuations of the Tarim Basin groundwater surface elevation. Complete desiccation of Lop Nor was achieved two decades prior to the initiation of industrial-grade irrigation in the A.D. 1960s and A.D. 1970s.

Fig. A2. Total annual precipitation climatology (A.D. 1979—2000) from MERRA for the same domain as shown in Fig. A1 (Panel A). MERRA predicts at least twice the amount of annual precipitation across mountains adjacent to the Tarim Basin as compared to WorldClim.
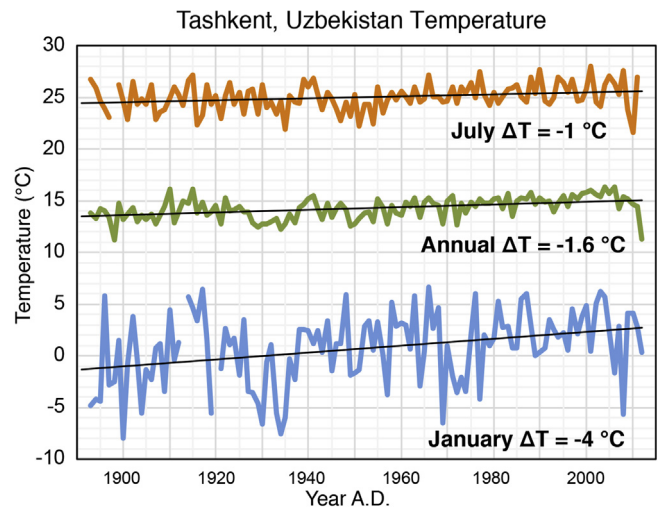
Fig. A3. Summer (top), winter (bottom), and mean annual (middle) temperature recorded at a meteorological station in Tashkent, Uzbekistan (41.33°N, 69.30°E at 477 m a.s.l.). Middle 19th century cooling relative to modern climate is determined from the linear trends. Data from the Global Historical Climatology Network (GHCN) Version 2 database.

Fig. A1. Panel A: Total annual precipitation climatology (A.D. 1950—2000) from WorldClim, depicted here across the Tibetan Plateau and the Tarim Basin. WorldClim erroneously predicts hyperarid conditions over the Kunlun mountains (Panel B), which sustain significant glacier systems and thus imply greater precipitation amounts than depicted by WorldClim. Bottom image from Google Earth™.
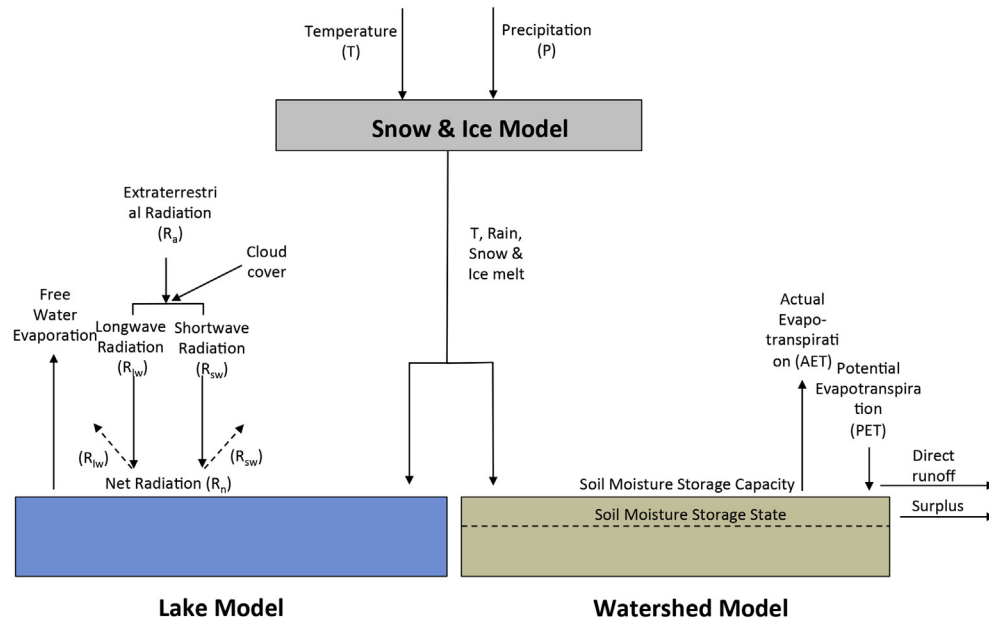
Fig. A4. Schematic of the three models used in this study.

Table A1
^{14}C age and significance of subfossil organic matter in the Tarim Basin.

Location	Field label	Dated material	AMS number	δ^{13}C (‰)	^{14}C age (yrs BP)±1σ	Year AD±1σ	Significance
Taklamakan Desert							
Site 1 (40.32 °N, 80.10 °E)	TD-10-08	*P. euphratica* wood	ETH-40752	−25.0	525 ± 30	1402 ± 33	Date on wind-abraded outermost preserved rings of stump rooted (in growth position) in waterlain sediments. Indicates period when water table was sufficiently high to permit growth and survival of *P. euphratica*.
	TD-10-03a	Wood fragment	ETH-41902	−24.3	105 ± 40	1816 ± 80	Age of reworked wood fragment entrained in stratified sandy silt. Dates deposition of waterlain sediments, when water table was expressed above ground surface.
	TD-10-03b	Wood fragment	ETH-41903	−27.8	275 ± 40	1607 ± 87	Age of reworked wood fragment entrained in stratified sandy silt. Dates deposition of waterlain sediments, when water table was expressed above ground surface.
	TD-10-03c	Wood fragment	ETH-41904	−25.4	90 ± 40	1820 ± 79	Age of reworked wood fragment entrained in stratified sandy silt. Dates deposition of waterlain sediments, when water table was expressed above ground surface.
	TD-10-03d	Wood fragment	ETH-41905	−24.4	235 ± 40	1718 ± 111	Age of reworked wood fragment entrained in stratified sandy silt. Dates deposition of waterlain sediments, when water table was expressed above ground surface.
	TD-10-03e	Wood fragment	ETH-41906	−25.4	95 ± 40	1818 ± 79	Age of reworked wood fragment entrained in stratified sandy silt. Dates deposition of waterlain sediments, when water table was expressed above ground surface.
	TD-10-05 (outer)	*P. euphratica* wood	ETH-41907	−25.1	105 ± 40	1816 ± 80	Date on wind-abraded outermost preserved rings of stump rooted (in growth position) in waterlain sediments. Indicates when water table was sufficiently high to permit growth and survival of *P. euphratica* tree.
	TD-10-06 (inner)	*P. euphratica* wood	ETH-41908	−26.0	115 ± 40	1813 ± 81	Date on innermost preserved rings of stump (same as TD-10-05) rooted (in

(*continued on next page*)

Table A1 (continued)

Location	Field label	Dated material	AMS number	δ^{13}C (‰)	^{14}C age (yrs BP)±1σ	Year AD±1σ	Significance
							growth position) in waterlain sediments. Indicates when water table was sufficiently high to permit growth and survival of sapling *P. euphratica* tree.
	TD-10-09	*P. euphratica* wood	ETH-41909	−26.3	500 ± 40	1415 ± 33	Date on wind-abraded outer preserved wood of stump rooted (in growth position) in waterlain sediments. Indicates period when water table was sufficiently high to permit growth and survival of *P. euphratica*.
	TD-10-10	*P. euphratica* wood	ETH-40753	−24.3	455 ± 30	1442 ± 20	Date on wind-abraded outer preserved wood of log resting on waterlain sediments. Log is assumed to articulate with stump of TD-10-09, less than one meter away. Indicates period when water table was sufficiently high to permit growth and survival of *P. euphratica*.
	TD-14C-10 (outer)	*P. euphratica* wood	UCIAMS-112536	−24.2	530 ± 20	1407 ± 25	Outermost rings from same log as TD-10-10. Sample used together with TD-14C-10 (inner) to refine age of sapling recruitment.
	TD-14C-10 (inner)	*P. euphratica* wood	UCIAMS-112537	−22.7	625 ± 20	1345 ± 32	Innermost rings from same log as TD-10-10. Sample used together with TD-14C-10 (inner) to refine age of sapling recruitment. Represents close age for tree recruitment, and hence when the water table must have been at ground surface to permit germination and survival of sapling *P. euphratica*.
	TD-14C-7 (outer)	*P. euphratica* wood	UCIAMS-112543	−24.0	495 ± 20	1427 ± 9	Outermost rings from *P. euphratica* stump rooted (in growth position) in waterlain sediments. Sample used together with TD-14C-7 (inner) to refine age of sapling recruitment.
	TD-14C-7 (inner)	*P. euphratica* wood	UCIAMS-112543	−24.0	675 ± 20	1321 ± 40	Innermost rings from *P. euphratica* stump rooted (in growth position) in waterlain sediments. Sample used together with TD-14C-7 (outer) to refine age of sapling recruitment. Represents close age for tree recruitment, and hence when the water table must have been at ground surface to permit germination and survival of sapling *P. euphratica*.
	TD-14C-12 (outer)	*P. euphratica* wood	UCIAMS-112538	−24.1	570 ± 25	1362 ± 35	Outermost rings from *P. euphratica* stump rooted (in growth position) in waterlain sediments. Sample used together with TD-14C-12 (inner) to refine age of sapling recruitment.
	TD-14C-12 (inner)	*P. euphratica* wood	UCIAMS-112539	−24.2	670 ± 20	1326 ± 40	Innermost rings from *P. euphratica* stump rooted (in growth position) in waterlain sediments. Sample used together with TD-14C-12 (outer) to refine age of sapling recruitment. Represents close age for tree recruitment, and hence when the water table must have been at ground surface to permit germination and survival of sapling *P. euphratica*.
Site 2 (40.09 °N, 80.99 °E)	TD-10-01 (recon)	*T. ramosissima* wood	ETH-40751	−23.7	600 ± 30	1350 ± 32	Reconnaisance date on middle rings of disarticulated *T. ramosissima* log resting on waterlain yardang surface. Indicates period when water table was sufficiently high to permit grouth and survival of *T. ramosissima*.
	TD-10-01 (inner)	*T. ramosissima* wood	ETH-41899	−26.3	800 ± 40	1228 ± 34	Date on innermost rings near pith of TD-10-01 log. Represents close age for tree recruitment, and hence when the water table must have been at ground surface to permit germination and survival of sapling *T. ramosissima*. Sample used together with TD-10-01

Table A1 (continued)

Location	Field label	Dated material	AMS number	δ¹³C (‰)	¹⁴C age (yrs BP)±1σ	Year AD±1σ	Significance
							(outer) and ring count to refine age of sapling recruiment.
	TD-01-01 (outer)	*T. ramosissima wood*	ETH-41900	−27.1	450 ± 40	1456 ± 43	Date on outermost preserved rings of TD-10-01 log. Sample used together with TD-10-01 (inner) and ring count to refine age of sapling recruitment.
	TD-10-02	*P. euphratica wood*	ETH-41901	−29.6	605 ± 40	1350 ± 34	Date on abraded outermost preserved rings of stump rooted in growth position in waterlain sediments. Indicates period when water table was sufficiently high to permit growth and survival of P. euphratica.
Site 3 (38.22 °N, 83.15 °E)	TD-14C-438-4	*P. euphratica wood*	ETH-43844	−23.7	235 ± 30	1722 ± 97	Date on abraded outermost preserved rings of stump rooted in growth position in waterlain sediments. Indicates period when water table was sufficiently high to permit growth and survival of P. euphratica.
	TD-14C-438-3	*P. euphratica wood*	ETH-46142	−21.9	365 ± 25	1537 ± 57	Date on sapwood (from beneath preserved bark) from stump rooted (in growth position) in waterlain sediments. Indicates period when water table was sufficiently high to permit last growth of P. euphratica tree.
	TD-14C-438-5	*P. euphratica wood*	ETH-46143	−21.6	310 ± 25	1568 ± 44	Date on sapwood (from beneath preserved bark) from stump rooted (in growth position) in waterlain sediments. Indicates period when water table was sufficiently high to permit last growth of P. euphratica tree.
	TD-14C-438_section	*P. euphratica wood fragment*	ETH-46147	−22.5	370 ± 25	1532 ± 58	Reworked wood fragment entrained in stratified sandy silt. Sample dates deposition of waterlain sediments, when water table was expressed above ground surface.
	TD-14C-438-1 (outer)	*P. euphratica wood*	UCIAMS-112540	−20.1	385 ± 20	1505 ± 56	Outermost rings from P. euphratica stump rooted (in growth position) in waterlain sediments. Sample used together with TD-14C-438-1 (inner) to refine age of sapling recruitment.
	TD-14C-438-1 (inner)	*P. euphratica wood*	UCIAMS-112541	−24.7	510 ± 20	1421 ± 12	Innermost rings from P. euphratica stump rooted (in growth position) in waterlain sediments. Sample used together with TD-14C-438-1 (outer) to refine age of sapling recruitment. Represents close age for tree recruitment, and hence when the water table must have been at ground surface to permit germination and survival of sapling P. euphratica.
	TD-14C-438-2 (outer)	*P. euphratica wood*	UCIAMS-112542	−23.9	470 ± 20	1435 ± 8	Outermost rings from P. euphratica stump rooted (in growth position) in waterlain sediments. Sample used together with TD-14C-438-2 (inner) to refine age of sapling recruitment.
	TD-14C-438-2 (inner)	*P. euphratica wood*	UCIAMS-112543	−23.4	670 ± 25	1328 ± 40	Innermost rings from P. euphratica stump rooted (in growth position) in waterlain sediments. Sample used together with TD-14C-438-1 (outer) to refine age of sapling recruitment. Represents close age for tree recruitment, and hence when the water table must have been at ground surface to permit germination and survival of sapling P. euphratica.
	TD-14C-438-R1a	*Phragmites sp. stem*	ETH-46148	−22.3	815 ± 25	1227 ± 24	Phragmites sp. (reed) stem rooted in waterlain sediment buried beneath sand dune. Age indicates timing of sediment deposition, and hence when water table was expressed above ground surface.
	TD-14C-438-R1b	*Phragmites sp. stem*	ETH-46612	−24	855 ± 25	1187 ± 36	Phragmites sp. (reed) stem rooted in waterlain sediment buried beneath

Table A1 (continued)

Location	Field label	Dated material	AMS number	δ^{13}C (‰)	^{14}C age (yrs BP)±1σ	Year AD±1σ	Significance
							sand dune. Age indicates timing of sediment deposition, and hence when water table was expressed above ground surface.
	TD-14C-438-R1c	*Phragmites* sp. stem	ETH-46613	−20.5	824 ± 25	1219 ± 26	Phragmites sp. (reed) stem rooted in waterlain sediment buried beneath sand dune. Age indicates timing of sediment deposition, and hence when water table was expressed above ground surface.
	TD-14C-438-R1d	*Phragmites* sp. stem	ETH-46614	−21.1	820 ± 25	1223 ± 25	Phragmites sp. (reed) stem rooted in waterlain sediment buried beneath sand dune. Age indicates timing of sediment deposition, and hence when water table was expressed above ground surface.
Site 4 (40.36 °N, 84.32 °E)	TD-14C-171-P2	P. euphratica wood	ETH-43843	−26.4	120 ± 30	1814 ± 80	Date on sapwood (from beneath preserved bark) from stump rooted (in growth position) in waterlain sediments. Indicates period when water table was sufficiently high to permit last growth of *P. euphratica* tree.
	TD-14C-171-P1	P. euphratica wood	ETH-46144	−24.4	75 ± 25	1830 ± 77	Date on sapwood (from beneath preserved bark) from stump rooted (in growth position) in waterlain sediments. Indicates period when water table was sufficiently high to permit last growth of *P. euphratica* tree.
	TD-14C-171-P1r	P. euphratica wood	ETH-46145	−23.8	80 ± 25	1828 ± 77	Replicate of TD-14C-171-P1
	TD-14C-171-P3	P. euphratica wood	ETH-46146	−27.1	60 ± 25	1839 ± 76	Date on sapwood (from beneath preserved bark) from stump rooted (in growth position) in waterlain sediments. Indicates period when water table was sufficiently high to permit last growth of *P. euphratica* tree.
Lop Desert Site 5 (39.71 °N, 89.92 °E)	LN-10-01a	Bivalve shell fragment	ETH-40754	−4.2	490 ± 35	1424 ± 23	Shell fragment in lakebed sediments located ~10 km north/inboard of 815 m shoreline. Shell dates to when the level of palaeolake Lop Nor stood at or very close to the 815 m shoreline.
	LN-10-01b	Gastropod shell	ETH-41910	−6.2	520 ± 45	1395 ± 41	Shell in lakebed sediments located ~10 km north/inboard of 815 m shoreline. Shell dates to when the level of palaeolake Lop Nor stood at or very close to the 815 m shoreline.
	LN-10-02a	Bivalve shell	ETH-40755	−2.0	375 ± 35	1532 ± 59	Shell in lakebed sediments located ~10 km north/inboard of 815 m shoreline. Shell dates to when the level of palaeolake Lop Nor stood at or very close to the 815 m shoreline.
	LN-10-02b	Bivalve shell	ETH-41911	−9.3	845 ± 45	1182 ± 57	Shell in lakebed sediments located ~10 km north/inboard of 815 m shoreline. Shell dates to when the level of palaeolake Lop Nor stood at or very close to the 815 m shoreline.
	LN-10-02c	Bivalve shell	ETH-41912	−9.0	410 ± 45	1508 ± 62	Shell in lakebed sediments located ~10 km north/inboard of 815 m shoreline. Shell dates to when the level of palaeolake Lop Nor stood at or very close to the 815 m shoreline.
	LN-10-02d	Bivalve shell	ETH-41912	−6.2	530 ± 45	1387 ± 42	Shell in lakebed sediments located ~10 km north/inboard of 815 m shoreline. Shell dates to when the level of palaeolake Lop Nor stood at or very close to the 815 m shoreline.

Table A2
Dendrochronologically refined 14C ages of select *P. euphratica* and *T. ramosissima* sp. in the Taklamakan Desert. Numbers in bold are recruitment dates.

Dated material	AMS number	14C age (yrs BP) ± 1σ	Ring count	Modeled date (Year AD) ± 1σ
P. euphratica wood	UCIAMS-112537 (inner)	625 ± 20	42	**1369 ± 18**
	UCIAMS-112536 (outer)	530 ± 20		1411 ± 18
P. euphratica wood	UCIAMS-112543 (inner)	675 ± 20	67	**1368 ± 5**
	UCIAMS-112543 (outer)	495 ± 20		1435 ± 5
P. euphratica wood	UCIAMS-112539 (inner)	670 ± 20	35	**1323 ± 38**
	UCIAMS-112538 (outer)	570 ± 25		1358 ± 38
T. ramosissima wood	ETH-41899 (inner)	800 ± 40	146	**1268 ± 17**
	ETH-41900 (outer)	450 ± 40		1414 ± 17
P. euphratica wood	UCIAMS-112541 (inner)	510 ± 20	78	**1420 ± 9**
	UCIAMS-112540 (outer)	385 ± 20		1498 ± 9
P. euphratica wood	UCIAMS-112543 (inner)	670 ± 25	59	**1375 ± 5**
	UCIAMS-112542 (outer)	470 ± 20		1434 ± 5

Table A3a
Timeline of the Mongol Empire (from Atwood, 2004).

Event	Year(s) A.D.	Notes
Unification of Tribes in Mongolia	1206	
First attack on the Tanguts (Xi Xia)	1209	
First campaign in north China (Qin)	1211	
Campaigns in Manchuria/Korea	1211–1215	
Jebe Noyon's pursuit of Guchluq (Tarim Basin to Kashgar)	1218	
War against the Kwarazm Shah	1219–1220	
Campaign into Afghanistan to the Indus	1221	
Subödei and Jebe's ride (Samarkand – Tehran – Tabriz – Khalka River – Kiev – Bulgar – Lake Balkhash)	1221–1224	
Final subjugation of the Tanguts (Xi Xia)	1226–1227	
Death of Chinggis Khan	1227	
Conquest of Qin (North China)	1231–1234	
Conquest of Korea	1231	
Conquest of Iran and Georgia	1231–1236	
Conquest of Russia, Hungary, Poland	1236–1241	*A.D. 1241 marks the largest areal extent of the Mongol Empire
Conquest of Tibet	1240	
Conquest of Sung (South China)	1252–1259	
Conquest of Iraq and Syria	1256–1288	
Attacks on Japan	1274	
	1281	
Conquest of Vietnam	1283	
Conquest of Burma	1287	
Death of Kublai Khan	1294	

Table A3b
Chronology of the Mongol Empire and Khanate successor nations.

Durations of reign: Mongols and successors	Established	Disestablished
Mongol Empire	1206	1294
Ilkhanate	1256	1335
Golden Horde	1241	1502
Khanate of Chaghadai	1225	1687
Timurid Dynasty	1370	1507
Mughal Empire	1526	1857
Crimean Khanate	1441	1783
Dzunghar Khanate	1634	1758

References

Aizen, V.B., Aizen, E.M., Melack, J.M., 1995. Climate, snow cover, glaciers and runoff in the Tien Shan, Central Asia. Water Resour. Bull. 31 (6), 1113–1129.

Allen, R.G., Pereira, L.S., Raes, D., Smith, M., 1998. Crop Evapotranspiration – Guidelines For Computing Crop Water Requirements, Food and Agriculture Organization of the United States, Irrigation and Drainage, paper 56, Rome, Italy.

Alley, W.M., 1984. On the treatment of evapotranspiration, soil moisture accounting, and aquifer recharge in monthly water balance models. Water Resour. Res. 20, 1137–1149.

Atwood, C.P., 2004. Encyclopedia of Mongolia and the Mongol Empire. Facts on File, Inc., New York.

Barclay, D.J., Wiles, G.C., Calkin, P.E., 2009. Holocene glacier fluctuations in Alaska. Quat. Sci. Rev. 28, 2034–2048.

Barclay, D.J., Yager, E.M., Graves, J., Kloczko, M., Calkin, P.E., 2013. Late Holocene glacial history of the Copper River Delta, coastal south-central Alaska, and controls on valley glacier fluctuations. Quat. Sci. Rev. 81, 74–89.

Barth, C., 2013. Toward the Use of Modern Modeling Tools in Paleoclimate Studies. University of Nevada, Reno, 121 pp.

Barzagur, D., 2002. Territorial organization of Mongolian pastoral livestock husbandry in the transition to a market economy. Focus Geogr. 47 (1), 20–25.

Berghuijs, W.R., Woods, R.A., Hrachowitz, M., 2014. A precipitation shift from snow towards rain leads to a decrease in streamflow. Nat. Clim. Change 4, 583–586.

Birkel, S.D., et al., 2012. Climate inferences from a glaciological reconstruction of the late Pleistocene Wind River Ice Cap, Wind River Range, Wyoming. Arct. Antarct. Alp. Res. 44 (3), 265–276.

Blard, P.-H., et al., 2011. Lake highstands on the Altiplano (Tropical Andes) contemporaneous with Heinrich 1 and the Younger Dryas: new insights from ^{14}C, U–Th dating and δ^{18}O of carbonates. Quat. Sci. Rev. 30, 3973–3989.

Bosson, J., 2013. Mongolia: Heartland of Asia. In: Fitzhugh, W.W., Rossabi, M., Honeychurch, W. (Eds.), Genghis Khan and the Mongol Empire. Arctic Studies Center, Smithsonian Institution & Mongolian Preservation Foundation, Washington, p. 314.

Braithwaite, R.J., Olesen, O.B., 1989. Calculation of glacier ablation from air temperature, West Greenland. In: Oerlemans, J. (Ed.), Glacier Fluctuations. D. Reidel Publishing Company, Dordrecht, p. 160.

Broecker, W.S., Putnam, A.E., 2013. Hydrologic impacts of past shifts of Earth's thermal equator offer insight into those to be produced by fossil fuel CO_2. Proc. Natl. Acad. Sci. 110 (42), 16710–16715.

Bronk Ramsay, C., 2009. Bayesian analysis of radiocarbon dates. Radiocarbon 51 (1), 337–360.

Bronk Ramsay, C., 2011. Development of the radiocarbon calibration program Oxcal. Radiocarbon 43 (2A), 255–363.

Buckley, B.M., et al., 2010. Climate as a contributing factor in the demise of Angkor, Cambodia. Proc. Natl. Acad. Sci. 107, 6748–6752.

Chen, F., Xiaozhong, H., Zhang, J., Holmes, J.A., Chen, J., 2006a. Humid Little Ice Age in arid central Asia documented by Bosten Lake, Xinjiang, China. Sci. China Ser.

D 49 (12), 1280—1290.

Chen, Y., Takeuchi, K., Changchun, X., Chen, Y., Xu, Z., 2006b. Regional climate change and it effects on river runoff in the Tarim Basin, China. Hydrol. Process. 20, 2207—2216.

Chiang, J.C.H., Friedman, A.R., 2012. Tropical cooling, interhemispheric thermal gradients, and tropical climate change. Annu. Rev. Earth Planet. Sci. 40, 383—412.

Chiang, J.C.H., et al., 2015. Role of seasonal transitions and westerly jets in East Asian Paleoclimate. Quat. Sci. Rev. 108, 111—129.

Cook, E.R., et al., 2010. Asian monsoon failure and megadrought during the Last Millennium. Science 328, 486—489.

Cook, E.R., Kairiukstis, L., 1990. Methods of Dendrochronology in Applications in the Environmental Sciences. Kluwer, Dordrecht, 394 pp.

Curtin, J., 1908. The Mongols, a History. Little, Brown and Co., Boston.

Davi, N.K., et al., 2015. A long-term context (931 — 2005 C.E.) for rapid warming over Central Asia. Quat. Sci. Rev. 121, 89—97.

Denton, G.H., Broecker, W.S., 2008. Wobbly ocean conveyor circulation during the Holocene? Quat. Sci. Rev. 27 (21—22), 1939—1950.

Denton, G.H., Karlén, W., 1973. Holocene climatic variations — their pattern and possible cause. Quat. Res. 3, 155—205.

Dettinger, M., 2014. Climate change: impacts in the third dimension. Nat. Geosci. 7, 166—167.

Dughlát, M.H., 1544. The Tarikh-i-Rashidi: a History of the Moghuls of Central Asia. Adamant Media Corporation, 692 pp.

Enzel, Y., et al., 2003. Late Holocene climates of the Near East deduced from Dead Sea level variations and modern regional winter rainfall. Quat. Res. 60, 263—273.

Fitzhugh, W.W., 2013. Genghis Khan: empire and legacy. In: Fitzhugh, W.W., Rossabi, M., Honeychurch, W. (Eds.), Genghis Khan and the Mongol Empire. Arctic Studies Center, Smithsonian Institution & Mongolian Preservation Foundation, Washington, p. 314.

Friedman, A.R., Hwang, Y.-T., Chiang, J.C.H., Frierson, D.M.W., 2013. Interhemispheric temperature asymmetry over the 20th century and future projections. J. Clim. 26, 5419—5433.

Gries, D., et al., 2003. Growth and water relations of *Tamarix ramosissima* and *Populus euphratica* on Taklamakan desert dunes in relation to depth to a permanent water table. Plant Cell Environ. 26, 725—736.

Grove, J.M., 2001. The initiation of the "Little Ice Age" in regions round the North Atlantic. Clim. Change 48, 53—82.

Haghani, S., et al., 2015. An early 'Little Ice Age' brackish water invasion along the south coast of the Caspian Sea (sediment of Langarud wetland) and its wider impacts on environment and people. Holocene. http://dx.doi.org/10.1177/0959683615596835.

Hamon, W.R., 1961. Estimating the potential evapotranspiration. J. Hydraul. Div. Proc. Am. Soc. Civ. Eng. 87, 107—120.

Hedin, S.A., 1940. The Wandering Lake. Routeledge, New York.

Hijmans, R., Cameron, S.E., Parra, J.L., Jones, P.G., Jarvis, A., 2005. Very high resolution interpolated climate surfaces for global land areas. Int. J. Climatol. 25, 1965—1978.

Holzhauser, H., Magny, M., Zumbühl, H.J., 2005. Glacier and lake-level variation in west-central Europe over the last 3500 years. Holocene 15, 789—801.

Hongfei, Z., Yudong, S., Shunjun, H., 2000. Irrigated Agriculture and Sustainable Water Management Strategies in the Tarim Basin: New Approaches to Water Management in Central Asia, Aleppo, Syria, pp. 127—138.

Hörner, N.G., Chen, P.C., 1935. Alternating lakes. Some river changes and lake displacements in Central Asia. Geogr. Ann. 17, 145—166.

Huntington, E., 1907. Lop-Nor. A Chinese Lake. Part 1. The unexplored Salt Desert of Lop. Bull. Am. Geogr. Soc. 39 (2), 65—77.

Jenkins, G., 1974. A note on climatic cycles and the rise of Chinggis Khan. Central Asiatic J. 18, 217—226.

Jensen, M.E., Burman, R.D., Allen, R.G., 1990. Evapotranspiration and Irrigation Water Requirements: a Manual. American Society of Civil Engineers, manuals and reports on engineering practice, 70, 332 pp.

Kalnay, E., et al., 1996. The NCEP/NCAR 40-yr reanalysis Project. Bull. Am. Meteorological Soc. 77 (3), 437—471.

Kozloff, P.K., 1898. The Lob-Nor controversy. Geogr. J. 11 (6), 652—658.

Lamb, H.H., 1979. Climatic variation and changes in the wind and ocean circulation: the Little Ice Age in the northeast Atlantic. Quat. Res. 11 (1), 1—20.

Lattimore, O., 1938. The geographical factor in Mongol history. Geogr. J. 91, 1—16.

Legates, D.R., McCabe, G.J., 2005. A re-evaluation of the average annual global water balance. Geogr. Rev. 82, 253—267.

Li, B.G., et al., 2008. High precision topographic data on Lop Nor basin's lake "Great Ear" and the timing of its becoming a dry salt lake. Chin. Sci. Bull. 53 (6), 905—914.

Li, J., Yuan, Y., Zhou, W., 1989. In: Studies of Tree-ring Climatology and Hydrology in Xinjiang Province. China Meterological Press, Beijing (in Chinese).

Liu, W., Liu, Z., An, Z., Wang, X., Chang, F., 2010. Wet climate during the 'Little Ice Age' in the arid Tarim Basin, northwestern China. Holocene 21, 409—416.

Lowell, T.V., et al., 2013. Late olocene expansion of Istorvet ice cap, Liverpool Land, east Greenland. Quat. Sci. Rev. 63, 128—140.

Luce, C.H., Abatzoglou, J.T., Holden, Z.A., 2014. The Missing mountain water: slower westerlies decrease orographic enhancement in the Pacific Northwest USA. Science 342 (6164), 1360—1364.

Luckman, B.H., 2000. The Little Ice Age in the Canadian Rockies. Geomorphology 32, 357—384.

McCabe, G.J., Hay, L.E., Bock, A., Markstrom, S.L., Atkinson, R.D., 2015. Inter-annual and spatial variability of Hamon potential evapotranspiration model coefficients. J. Hydrol. 521, 389—394.

McCabe, G.J., Markstrom, S.L., 2007. A Montly Water Balance Model Driven by a Graphical User Interface.

McKinnon, K.A., Huybers, P., 2014. On using the seasonal cycle to interpret extratropical temperature changes since 1950. Geophys. Res. Lett. 41, 4676—4684.

McKinnon, K.A., Stine, A., Huybers, P., 2013. The spatial structure of the annual cycle in surface temperature: amplitude, phase, and Lagrangian history. J. Clim. http://dx.doi.org/10.1175/JCLI-D-13-0021.1.

Mood, B.J., Smith, D.J., 2015. Latest Pleistocene and Holocene behaviour of Franklin Glacier, Mr. Waddington area, British Columbia Coast Mountains, Canada. Holocene. http://dx.doi.org/10.1177/0959683615569321.

Nagashima, K., et al., 2011. Millennial-scale oscillations of the westerly jet path during the last glacial period. J. Asian Earth Sci. 40, 1214—1220.

Nicolussi, K., Patzelt, G., 2001. Untersuchungen zur holozänen Gletscherentwicklung von Pasterze und Gepatschferner (Ostalpen). Z. für Gletscherkd. Glazialgeol. 36, 1—87.

Pausata, F.S.R., Battisti, D.S., Nisancioglu, K.H., Bitz, C.M., 2011. Chinese stalagmite ^{18}O controlled by changes in the Indian Monsoon during a simulated Heinrich event. Nat. Geosci. 4, 474—480.

Pederson, N., Hessl, A.E., Baatarbileg, N., Anchukaitis, K.J., Di Cosmo, N., 2014. Pluvials, droughts, and the Mongol Empire, and modern Mongolia. Proc. Natl. Acad. Sci. http://dx.doi.org/10.1073/pnas.1318677111.

Poppe, N., 1955. Renat's Kalmuck maps. Imago Mundi 12, 157—159.

Prejevalsky, N., 1879. From Kulja, across the Tien Shan to Lob-Nor. Marston. Searle, & Rivington, London.

Priestley, C.H.B., Taylor, R.J., 1972. On the assessment of surface heat flux and evaporation using large-scale parameters. Mon. Weather Rev. 100, 81—92.

Putnam, A.E., et al., 2013. The last glacial maximum at 44°S documented by a ^{10}Be moraine chronology at Lake Ohau, Southern Alps of New Zealand. Quat. Sci. Rev. 62, 114—141.

Reimer, P.J., et al., 2013. IntCal13 and Marine13 radiocarbon age calibration curves 0—50,000 years cal BP. Radiocarbon 55, 1869—1887.

Rienecker, M.M., et al., 2011. MERRA — NASA's modern-era retrospective analysis for research and applications. J. Clim. 24, 3624—3648.

Rossabi, M., 1994. All the Khan's horses. Nat. Hist. 103 (10), 48—57.

Ryder, J.M., Thompson, B., 1986. Neoglaciation in the southern Coast Mountains of British Columbia: chronology prior to the late Neoglacial maximum. Can. J. Earth Sci. 23, 273—287.

Solomina, O., Barry, R., Bodnya, M., 2004. The retreat of Tien Shan glaciers (Kyrgyzstan) since the Little Ice Age estimated from aerial photographs, lichenometric and historical data. Geogr. Ann. 86A (2), 205—215.

Solomon, S., et al., 2007. IPCC Fourth Assessment Report: Climate Change 2007: Climate Change 2007: Working Group I: the Physical Science Basis. Cambridge University Press, New York.

Stein, A., 1903. Sand-buried Ruins of Khotan. T. Fisher Unwin, London.

Thevs, N., 2011. Water scarcity and allocation in the Tarim Basin: Decision structures and adaptations on the local level. J. Curr. Chin. Aff. 3, 113—137.

Thevs, N., Zerbe, S., Gahlert, F., Mijit, M., Succow, M., 2007. Productivity of reed (*Phragmites australis* Trin. ex Steud.) in continental-arid NW China in relation to soil, groundwater, and land-use. J. Appl. Bot. Food Qual. 81, 81—62.

Thornthwaite, C.W., 1948. An approach toward a rational classification of climate. Geogr. Rev. 38, 55—94.

Tonybee, A.J., 1934. A study of history. In: The Growths of Civilizations, vol. 3. Oxford University Press.

Winter, T.C., Rosenberry, D.O., Sturrock, A.M., 1995. Evaluation of eleven equations for determining evaporation for a small lake in the north central United States. Water Resour. Res. 31, 983—993.

Wolock, D.M., McCabe, G.J., 1999. Effects of potential climatic change on annual runoff in the coterminous United States. J. Am. Water Resour. Assoc. 35, 1341—1350.

Wolock, D.M., McCabe, G.J., Tasker, G.D., Moss, M.E., 1993. Effects of climate change on water resources in the Delaware River Basin. J. Am. Water Resour. Assoc. 29, 475—486.

Xu, Y., Ramanathan, V., 2012. Latitudinally asymmetric response of global surface temperature: implications for regional climate change. Geophys. Res. Lett. 39, L13706.

Yang, X., 1991. Geomorphologische Untersuchungen in Trockenraeumen NW-Chinas unter besonderer Beruecksichtigung von Badanjilin und Takelamagan. Goettinger Geogr. Abh. 96, 1—124.

Yang, X., Liu, Z., Zhang, F., White, P.D., Wang, X., 2006. Hydrological changes and land degradation in the southern and eastern Tarim Basin, Xinjiang, China. Land Degrad. Dev. 17, 381—392.

Yang, X., Zhu, Z., Jaekel, D., Owen, L.A., Han, J., 2002. Late Quaternary palaeoenvironmental change and landscape evolution along the Keriya River, Xinjiang, China: the relationship between high mountain glaciation and landscape evolution in foreland desert regions. Quat. Int. 97—98, 155—166.

Zhang, P.Z., et al., 2008. A test of climate, sun, and culture relationships from an 1810-year Chinese Cave record. Science 322 (5903), 940—942.

Zomer, R.J., et al., 2007. Trees and Water: Smallholder Agroforestry on Irrigated Lands in Northern India. International Water Management Institute, Colombo, Sri Lanka.

Zomer, R.J., Trabucco, A., Bossio, D.A., van Straaten, O., Verchot, L.V., 2008. Climate change mitigation: a spatial analysis of global land suitability for clean development mechanism afforestation and reforestation. Agric. Ecosyst. Environ. 126, 67—80.